R. & M. No. 3045
(18,098)
A.R.C. Technical Report

MINISTRY OF SUPPLY

AERONAUTICAL RESEARCH COUNCIL
REPORTS AND MEMORANDA

Calculated Velocity Distributions and Force Derivatives for a Series of High-Speed Aerofoils

By
C. S. SINNOTT, B.Sc.,
of the Aerodynamics Division, N.P.L.

LONDON: HER MAJESTY'S STATIONERY OFFICE
1957
NINE SHILLINGS NET

Calculated Velocity Distribution and Force Derivatives for a Series of High-Speed Aerofoils

By

C. S. SINNOTT, B.Sc.,
of the Aerodynamics Division, N.P.L.

*Reports and Memoranda No. 3045**

December, 1955

Summary.—The Polygon method of Woods[2] is used to calculate the velocity distribution over a number of two-dimensional aerofoils at low incidence, subcritical flows only being considered. Lift slopes and aerodynamic centres at zero lift are also calculated.

Some comparisons with experimental results are made, and these show good agreement at zero incidence.

1. *Introduction.*—A series of tests on a number of high-speed aerofoil sections is being undertaken by the High Speed Laboratory of the Aerodynamics Division, National Physical Laboratory. In this report some theoretical results for these aerofoils are presented and discussed.

The ' Polygon ' method of Woods[1] (1950) is used as this theory has previously been shown to give satisfactory results at high subsonic Mach numbers in the absence of local regions of supersonic flow. Application of the method is fully described by Woods in Ref. 2; physically it involves the replacement of an aerofoil by a finite number of circular arcs, on each of which it is assumed that the product of the radius of curvature and the velocity is constant. A further approximation, necessary to linearize the compressible-flow equation, is discussed in section 2.2.

Calculations have been made, for symmetric aerofoils of 10, 6 and 4 per cent thickness, derived from two basic sections, the RAE 102 and 104 ' rooftop ' aerofoils whose co-ordinates are given in Ref. 3 (Pankhurst and Squire, 1952). The completed programme is given in section 3.

Solutions for incompressible flow and for a Mach number of 0·70 have been obtained for each aerofoil at incidences of 0, 1, 2 and 4 deg. Velocity distributions for the thinner aerofoils are given at higher Mach numbers, but in no instance is the estimated critical Mach number of the aerofoil at zero incidence exceeded. In cases where the velocity increments due to incidence lead to supersonic flow the remaining subsonic part of the distribution is calculated; this may have little significance if the supersonic region in the corresponding real flow terminates in a shock wave.

The velocity distributions, which are obtained directly as the results of the Polygon method, are given in Tables 2 to 5; the curves of C_p or p/p_0 against x/c shown in Figs. 3 to 14 are derived from these by graphical methods. The results are discussed in Sections 4 and 5.

Comparisons with measured pressure distributions for the 6 per cent RAE 104 aerofoil are shown in Figs. 23, 24 and 25, and for the 10 per cent RAE 102 aerofoil in Fig. 26. The results for the latter aerofoil at zero Mach number and incidence are also compared with those given in Ref. 3; some comments on this comparison will be found in section 4.

* Published with permission of the Director, National Physical Laboratory.

The velocity distributions have been used to calculate the lift slopes and aerodynamic centres for zero incidence and these results are shown in Table 6.

2. *Theory*.—2.1. *Derivation of Basic Equations*.—In this section a short account of the basic mathematical theory of the Polygon[1] method is given.

With δs and δn orthogonal, the equations of the two-dimensional flow of an inviscid compressible fluid may be written[4]:

$$\left.\begin{aligned} \frac{\partial \theta}{\partial n} + \frac{(1 - M^2)}{q} \cdot \frac{\partial q}{\partial s} &= 0 \\ \frac{\partial \theta}{\partial s} - \frac{1}{q}\frac{\partial q}{\partial n} &= 0 \end{aligned}\right\}, \qquad (1)$$

where (q, θ) defines the velocity vector. Take ∂s in the stream direction; then from the definition of the velocity potential and stream function, ϕ and ψ respectively, *viz.*,

$$d\phi = q\,ds\,,\; d\psi = \frac{\rho}{\rho_0} q\,dn\,,$$

equations (1) become:

$$\left.\begin{aligned} \frac{\partial \theta}{\partial \psi} + \frac{\rho_0}{\rho} \cdot \frac{\beta^2}{q} \cdot \frac{\partial q}{\partial \theta} &= 0 \\ \frac{\partial \theta}{\partial \phi} - \frac{\rho}{\rho_0} \cdot \frac{1}{q} \cdot \frac{\partial q}{\partial \psi} &= 0 \end{aligned}\right\} \qquad (2)$$

Put

$$dr = \beta\,dL\,, \qquad (3)$$

where

$$L = \log_e \frac{U}{q}\,,$$

and

$$m = \frac{\rho_0}{\rho} \cdot \beta\,. \qquad (4)$$

With these substitutions equations (2) may be written:

$$\left.\begin{aligned} \frac{\partial \theta}{\partial \psi} + m\frac{\partial r}{\partial \theta} &= 0 \\ \frac{\partial \theta}{\partial \phi} - \frac{1}{m}\frac{\partial r}{\partial \psi} &= 0 \end{aligned}\right\},$$

whence

$$\frac{\partial}{\partial \phi}\left(m\frac{\partial r}{\partial \phi}\right) + \frac{\partial}{\partial \psi}\left(\frac{1}{m}\frac{\partial r}{\partial \psi}\right) = 0\,.$$

This equation is linearized by replacing m by m_∞, its value in the free stream, which gives:

$$\frac{\partial^2 r}{\partial \psi^2} + m_\infty^2 \frac{\partial^2 r}{\partial \phi^2} = 0\,. \qquad (5)$$

A solution of equation (5) is derived as an integral equation, from which r can be evaluated for a particular aerofoil and Mach number by an iterative method. Incidence effects can then be calculated from the relation:

$$r_\alpha = r - \log_e \frac{\sin(\gamma + 2\alpha)/2}{\sin \gamma/2}, \quad \ldots \quad \ldots \quad \ldots \quad \ldots \quad (6)$$

where γ is a parameter defining position on the aerofoil.

The application of the method is described in Ref. 2, where quantities for the numerical solution of the derived integral equation are tabulated. The results of additional calculations for $M_\infty = 0\cdot70$, $0\cdot80$ and $0\cdot85$ are given in Table 1 of this paper.

2.2. *Discussion of the Approximation* $m = m_\infty$.—A point of interest arises from the approximation $m = m_\infty$, used to obtain the linearized equation (5). Although it would appear to be consistent to use this same degree of approximation in calculating the relation between q/U and r, it is not necessary to do so; for from equations (3) and (4):

$$r = \int_0^L m \frac{\rho}{\rho_0} \, dL, \quad \ldots \quad \ldots \quad \ldots \quad \ldots \quad \ldots \quad \ldots \quad (7)$$

which can be integrated exactly. However, von Kármán[5] (1941), when obtaining a compressible-flow solution in terms of the corresponding incompressible flow, defined r by:

$$r = m_\infty \int_0^L \frac{\rho}{\rho_0} \, . \, dL \, . \quad \ldots \quad \ldots \quad \ldots \quad \ldots \quad \ldots \quad (8)$$

Woods found that results obtained with equation (7) appeared to overestimate compressibility effects when compared with experiment, whereas those obtained with equation (8) underestimated the effects. He considered the two definitions by a comparison between a compressibility-correction formula derived from equation (7) and the well-known Kármán-Tsien rule. The comparison with experimental results led him to choose the definition:

$$r = \tfrac{1}{2} \int_0^L (m + m_\infty) \frac{\rho}{\rho_0} \, dL \, . \quad \ldots \quad \ldots \quad \ldots \quad \ldots \quad (9)$$

However, as is shown in Fig. 13 of Ref. 5, the Kármán-Tsien rule does not give the same results as equation (8), particularly at high Mach numbers. Moreover, a modification of the pressure distribution at zero Mach number by using such formulae implies no change in the equipotentials due to compressibility. Therefore, to examine thoroughly the value of the relations (7), (8) and (9) between q/U and r, all three have been used with the Polygon method to calculate the pressure distributions over a given aerofoil (6 per cent RAE 104) at Mach numbers of $0\cdot70$ and $0\cdot80$. The results are shown in Figs. 1 and 2 together with two sets of experimental results; these were obtained with transition from a laminar to turbulent boundary layer fixed near the leading edge, and with transition free. At $M_\infty = 0\cdot70$ the difference in the calculated pressure distributions due to the use of equations (7), (8) and (9) are small and less than measured boundary-layer effects. At $M_\infty = 0\cdot80$, however, the differences are significant and it appears that equation (9) gives the best agreement with the mean of the experimental results for zero incidence. Some results at incidence are also shown in Figs. 1 and 2 to illustrate the comparison of the three definitions of r for high values of C_p; they are not strictly comparable with the experimental results because viscous effects become important at non-zero lift.

The definition of r given by equation (9) has been used in all the calculations for this paper other than those discussed above. It does of course introduce an element of empiricism into the results, but this appears to be justified.

3. *Results.*—The following table gives the aerofoils and Mach numbers for which velocity distributions have been calculated by the Polygon method. In each case velocity distributions at 0, 1, 2 and 4 deg incidence are given in a separate table and curves of C_p or p/p_0 against x/c are drawn. The table below shows where these are to be found.

Summary of Calculations

Aerofoil	M_∞	Table	Figure
10 per cent RAE 102	0 0·70	2a 2b	3 4
6 per cent RAE 102	0 0·70 0·80	3a 3b 3c	5 6 7
6 per cent RAE 104	0 0·70 0·80	4a 4b 4c	8 9 10
4 per cent RAE 104	0 0·70 0·80 0·85	5a 5b 5c 5d	11 12 13 14

In addition to these results some have been taken from Ref. 2 for the 10 per cent RAE 104 aerofoil to illustrate thickness effects in Figs. 16, 17 and 18.

The plotted pressure-ratio distributions were calculated from the relations:

$$\left.\begin{aligned} C_p &= \left\{\left[1 - 0\cdot 2M_\infty^2\left(\left(\frac{q}{U}\right)^2 - 1\right)\right]^{3\cdot 5} - 1\right\}\Big/ 0\cdot 7M_\infty^2 \\ \frac{p}{p_0} &= \left(0\cdot 7M_\infty^2 C_p + 1\right)\Big/\left(1 + 0\cdot 2M_\infty^2\right)^{3\cdot 5} \end{aligned}\right\},$$

where the ratio of specific heats for air is taken as 1·4. The first relation was used to construct a graph of C_p versus q/U for a prescribed M_∞; values of C_p corresponding to the calculated velocities were then read off and p/p_0 calculated from the second equation.

Force derivatives were calculated from the velocity distributions at zero incidence by the method described in section 5 of Ref. 2. In Table 6 the lift and pitching-moment derivatives and aerodynamic centres are given for the aerofoils and Mach numbers listed above.

4. *Discussion and Analysis.*—4.1. *Pressure distributions.*—The pressure distribution curves of Figs. 3 to 14 show the effect of incidence for a given aerofoil and Mach number; all follow a similar pattern and call for little comment. It should be noted that for the curves where a supersonic peak is omitted, the remaining subsonic distribution is calculated on the assumption of shock-free flow. The designed 'roof-top' shape of the pressure distribution is evident, but the curves have not been drawn with discontinuous gradients at $0\cdot 4c$ for the RAE 102 and $0\cdot 6c$ for the RAE 104, where these aerofoil profiles have irregularities in curvature. To do so would imply a more exact solution than is given by the Polygon method, since an important feature of the method is the assumption of constant qc/UR over a selected number of discrete intervals of the chord. That the singularities have only a local effect is shown in Fig. 15 by the comparison for the 10 per cent RAE 102 aerofoil with results obtained in Ref. 3 by Goldstein's Approximation III. Measured pressure distributions are in any case modified by the boundary layer and show no discontinuities in gradient.

Figs. 16 and 17 show the effect of thickness on the pressure distributions for the RAE 104 profile at 0 and 2 deg incidence in incompressible flow. It is noticeable in Fig. 16 that, except in the neighbourhood of the leading and trailing edges, C_p is very nearly proportional to thickness at zero incidence; a similar relation is evident for $t/c < 0 \cdot 06$ in the p/p_0 curves of Fig. 18 at $M_\infty = 0 \cdot 70$.

Fig. 19 illustrates the effect of Mach number on the pressure distributions for the 4 per cent RAE 104 aerofoil at zero incidence, and Fig. 20 that at 2 degrees incidence. Some of these results and those for the 6 per cent RAE 104 aerofoil are presented in a different form in Fig. 21. Here C_p for a point on the upper surface of the aerofoils is plotted against Mach number. Curves for various values of C_{p0} are given by using the results for different incidences and aerofoil thicknesses. The first point of interest arises from curves D and E which compare the theoretical change in C_p with M_∞ for two different values of t/c at points on the aerofoils giving approximately the same C_{p0}. The similar variation with Mach number supports the remarks on thickness effect earlier in this section. Curves A, B and C are compared with values of C_p calculated from the approximate formula:

$$C_p = \frac{1}{\beta_\infty} C_{p0} - \frac{1}{2\beta_\infty^2}\left(1 - \beta_\infty + 0 \cdot 3 \frac{M_\infty^4}{\beta_\infty^2}\right) C_{p0}^2 + 0(C_{p0}^3) \,, \qquad \ldots \qquad \ldots \qquad (10)$$

which is derived in Ref. 2 on the basis of the semi-empirical relation between q/U and r given by equation (9) in section 2.2 of the present paper. These results are used to extrapolate curve C past $C_{p\,\mathrm{sonic}}$ so as to obtain an estimate of the critical Mach number for zero incidence. This is found to be $0 \cdot 846$, which compares well with the measured value of $0 \cdot 844$, but it should be noted that sonic velocity is first attained experimentally at $x = 0 \cdot 6c$. In Table 7 the value estimated from the Kármán-Tsien rule is $0 \cdot 853$; both this and the other values of M_{crit} given in Table 7 were estimated from the Polygon-method results for incompressible flow. The chief purpose of Fig. 21 is to show that the variation of C_p with M_∞ is similar for a considerable range of C_{p0} and independent of incidence, and that the approximate compressibility formula (10) compares well with the exact Polygon method for $M_\infty < (M_{\mathrm{crit}} - 0 \cdot 05)$.

A further comparison between the Polygon method and equation (10) is shown in Fig. 22. In this case the complete pressure distributions for the 4 per cent RAE 104 aerofoil at $\alpha = 0$ are given for $M_\infty = 0 \cdot 80$ and $0 \cdot 85$; results obtained by the Kármán-Tsien rule are also shown. Equation (10) slightly underestimates the results of the Polygon method at $M_\infty = 0 \cdot 85$, the Kármán-Tsien results being lower still; the difference in the shape of the pressure distributions at $M_\infty = 0 \cdot 85$ follows from the application of the compressibility rules to the calculated incompressible-flow pressure distribution. However, at $M_\infty = 0 \cdot 80$ differences introduced in this way are very small.

The preceding discussion of thickness and compressibility effects suggests a simple method for the estimation of compressible-flow pressure distributions for families of aerofoils:

(*a*) The use of the Polygon method to calculate the incompressible flow for one member of the family

(*b*) From (*a*) a linear relation with respect to thickness/chord ratio leads to values of C_{p0} for any (small) value of t/c

(*c*) Equation (10) may then be used to calculate the C_p distribution at a prescribed free-stream Mach number

(*d*) The function r (section 2) can be obtained from the values of C_p, and equation (6) used to estimate incidence effects. For this step it is sufficient to assume that the relation between the chordwise parameters γ and x/c is independent of thickness and Mach number.

Application of this scheme to aerofoils less than 10 per cent thick for Mach numbers less than $(M_{\mathrm{crit}} - 0 \cdot 05)$ should give results which do not differ significantly from those obtained by the exact Polygon method.

4.2. *Force Derivatives.*—In Fig. 27 the calculated lift shapes for the RAE 104 aerofoils are shown so as to illustrate the effects of thickness and Mach number. The derivative $\partial C_L/\partial\alpha$ is divided by $2\pi/\beta$ so that the quotient is a measure of thickness effect at a given Mach number or the effect of Mach number, in excess of that given by the Glauert law, at a given thickness.

The values of the position of the aerodynamic centre of the aerofoils, given as a fraction of the chord measured from the leading edge, vary little with thickness or Mach number. The results for the RAE 102 aerofoils show a slight forward movement with decrease in thickness or increase in Mach number; the same thickness effect is apparent from the RAE 104 values but these do not vary significantly with Mach number.

5. *Experimental Results for the* 6 *per cent RAE* 104 *and* 10 *per cent RAE* 102 *Aerofoils.*—Tests have been made on the 6 per cent RAE 104 aerofoil in the N.P.L. 20 × 8 in. High-Speed Tunnel*. As described in section 2.2 the results were found to justify the use of equation (9) in preference to equations (7) or (8). The comparison between theory and experiment is considered in more detail in this section, together with some low-speed results for the 10 per cent RAE 102 aerofoil[6].

Figs. 23, 24 and 25 show pressure distributions obtained by the Polygon method and by experiment for the 6 per cent RAE 104 aerofoil at $M_\infty = 0$, $0\cdot70$ and $0\cdot80$ respectively. The experimental results were obtained with transition fixed near the leading edge. In each case results for 0, 1 and 2 deg incidence are given. For incompressible flow there is good agreement between theory and experiment at zero incidence and this is confirmed by the comparison for the 10 per cent RAE 102 shown in Fig. 26. In the first place, Figs. 24 and 25 illustrate the conclusions of section 2.2, the curves for $\alpha = 0$ being the same as those in Figs. 1 and 2 derived from equation (9).

In all the results with the aerofoil producing lift the theory consistently overestimates the resultant pressure increments, particularly on the upper surface. This is to be expected, for the theory considers inviscid flow, so that thickening or separation of the boundary layer, with consequent loss of lift, is not allowed for. Woods[2] suggested an alternative interpretation of the theoretical results by supposing that the loss of lift could be represented by a change of incidence. He compared theory and experiment for the same total lift, defining an equivalent theoretical incidence α_E by:

$$\alpha_E = C_{L\,\mathrm{expt}}/(\partial C_L/\partial\alpha)_{\mathrm{Theory}}\ ;$$

but the experimental results which he used are no longer considered to be entirely satisfactory. A similar comparison can however be made for the 6 per cent RAE aerofoil from the measured C_L and values of $\partial C_L/\partial\alpha$ given in Table 6. The value of α_E corresponding to a real incidence of 1 deg at $M_\infty = 0\cdot70$ is $0\cdot76$ deg, and for 2 deg, $1\cdot58$ deg. Fig. 24 can now be reconsidered, for the theoretical pressure distribution at $\alpha = \alpha_E$ can be visualized by linear interpolation in the results for 0, 1 and 2 deg. It is clear that, whilst an improved comparison with experiment is obtained for the upper surface distribution, this is not the case for the lower surface. A probable explanation is that boundary-layer growth against the steep adverse pressure gradients on the upper surface is greater than on the lower surface. It appears that the loss in lift cannot be represented by an equivalent reduction in incidence.

6. *Concluding Remarks.*—It seems clear from the comparisons with experiment that the Polygon method is a satisfactory means of calculating subsonic flows about aerofoils when viscous effects are unimportant. It has been shown that the semi-empirical approximation embodied in equation (9) originally used by Woods is justified.

Perhaps the greatest value of this investigation lies in the suggested method of calculating approximate pressure distributions for geometrically similar aerofoils. For instance, calculations for a 10 per cent thick section in incompressible flow can be used to obtain pressure distributions

* The complete results are as yet unpublished.

for any similar section of smaller thickness at Mach numbers below ($M_{crit} - 0\cdot05$). Results obtained in this way should not differ significantly from those calculated by the exact Polygon method.

7. *Acknowledgements*.—The calculations for this paper were made by Mrs. J. S. Sindall and Miss J. E. Elliott of the Aerodynamics Division, N.P.L.

NOTATION

C_L		Lift coefficient
C_m		Pitching-moment coefficient, leading-edge axis
C_p		Pressure coefficient
C_{p0}		Pressure coefficient for incompressible flow
c		Aerofoil chord
h		Aerodynamic centre
L	$\equiv$	$\log_e (U/q)$
M		Local Mach number
m	$\equiv$	$\beta \rho_0/\rho$
p, p_0		Local and stagnation static pressure respectively
(q, θ)		Velocity vector in polar co-ordinates
r	$\equiv$	$\int_0^L \beta \, dL$
t		Maximum thickness of aerofoil
U		Speed of undisturbed stream
x		Distance measured along aerofoil chord from leading edge
α		Aerofoil incidence
β	$\equiv$	$\sqrt{(1 - M^2)}$
γ		Angular measure of chordwise distance (Ref. 2, Section 3)
ρ, ρ_0		Local and stagnation density respectively
ϕ		Velocity potential
ψ		Stream function
∞		Used as a suffix to denote values in the undisturbed stream

---

REFERENCES

No.	Author	Title, etc.
1	L. C. Woods	The two-dimensional subsonic flow of an inviscid fluid about an aerofoil of arbitrary shape. R. & M. 2811. November, 1950.
2	L. C. Woods	The application of the Polygon method to the calculation of the compressible subsonic flow round two-dimensional aerofoils. C.P. 115. June, 1952.
3	R. C. Pankhurst and H. B. Squire	Calculated pressure distributions for the RAE 100–104 aerofoil sections. C.P. 80. March, 1950.
	See also: J. Williams and E. M. Love ..	Surface slopes and curvatures of the RAE 100–104 and other rooftop-type aerofoil sections. C.P. 129. October, 1952.
4	H. W. Liepmann and A. E. Puchett	*Aerodynamics of a Compressible Fluid.* Chap. 11; Wiley and Sons. (1947).
5	T. von Kármán	Compressibility effects in aerodynamics. *J. Ae. Sci.* Vol. 8, No. 9. July, 1941.
6	H. C. Garner and A. S. Batson ..	Measurement of lift, pitching moment, pressure distribution and boundary layers on a 10 per cent RAE 102 aerofoil. (To be published.)

TABLE 1

q/U	$r \times 10^4$			q/U	$-r \times 10^4$		
	0·70	0·80	0·85		0·70	0·80	0·85
0·72	2573			1·00	0	0	0
0·73	2458			1·01	71	59	51
0·74	2345			1·02	140	117	101
0·75	2234			1·03	209	174	150
0·76	2125			1·04	276	229	197
0·77	2018			1·05	342	283	243
0·78	1912			1·06	406	335	287
0·79	1808			1·07	469	386	330
0·80	1707	1495	1359	1·08	532	435	371
0·81	1606	1405	1275	1·09	592	483	410
0·82	1509	1317	1194	1·10	653	530	447
0·83	1411	1231	1114	1·11	712	575	482
0·84	1317	1146	1036	1·12	770	619	516
0·85	1224	1063	960	1·13	827	661	547
0·86	1132	981	885	1·14	882	702	575
0·87	1042	901	812	1·15	935	741	
0·88	953	823	740	1·16	989	779	
0·89	866	746	670	1·17	1040	814	
0·90	780	671	601	1·18	1092	848	
0·91	696	597	534	1·19	1141	880	
0·92	613	525	469	1·10	1190	910	
0·93	532	454	405	1·21	1238		
0·94	452	385	342	1·22	1284		
0·95	373	317	281	1·23	1329		
0·96	296	251	222	1·24	1373		
0·97	220	186	164	1·25	1416		
0·98	146	123	108	1·26	1457		
0·99	72	61	53	1·27	1498		
1·00	0	0	0	1·28	1537		
				1·29	1575		
				1·30	1611		

Table of $r \left(\equiv \int_0^L \beta \, dL \right)$ against q/U

for $M_\infty = 0{\cdot}70,\ 0{\cdot}80$ and $0{\cdot}85$

TABLES 2a and 2b

Velocity Distributions

Table 2a

10 per cent RAE 102

$M_\infty = 0$

α	0 deg	1 deg		2 deg		4 deg	
x/c		Upper	Lower	Upper	Lower	Upper	Lower
0							
0·001	0·472	0·787	0·158	1·100		1·727	
0·006	0·908	1·101	0·704	1·310	0·505	1·710	0·101
0·017	1·038	1·174	0·901	1·312	0·762	1·585	0·485
0·032	1·075	1·175	0·971	1·277	0·883	1·478	0·668
0·053	1·101	1·181	1·020	1·261	0·940	1·418	0·778
0·084	1·118	1·179	1·051	1·241	0·993	1·362	0·868
0·136	1·127	1·174	1·080	1·222	1·032	1·315	0·935
0·200	1·133	1·170	1·091	1·208	1·056	1·282	0·978
0·272	1·132	1·160	1·101	1·194	1·070	1·254	1·006
0·350	1·130	1·150	1·104	1·181	1·078	1·230	1·024
0·432	1·118	1·139	1·091	1·160	1·075	1·200	1·030
0·517	1·093	1·111	1·071	1·128	1·058	1·161	1·021
0·603	1·067	1·081	1·050	1·095	1·037	1·121	1·007
0·687	1·040	1·052	1·030	1·063	1·016	1·084	0·992
0·760	1·015	1·024	1·007	1·033	0·996	1·050	0·976
0·837	0·995	1·000	0·990	1·008	0·980	1·021	0·964
0·896	0·975	0·980	0·971	0·985	0·964	0·994	0·952
0·946	0·952	0·962	0·952	0·959	0·945	0·965	0·935
0·981	0·923	0·926	0·926	0·926	0·918	0·929	0·921
0·998	0·864	0·870	0·862	0·865	0·862	0·864	0·859
1·000							

Table 2b

10 per cent RAE 102

$M_\infty = 0{\cdot}70$

α	0 deg	1 deg		2 deg		4 deg	
x/c		Upper	Lower	Upper	Lower	Upper	Lower
0							
0·001	0·472						
0·007	0·893						
0·017	1·056	0·870					
0·033	1·115	0·966		0·836			
0·053	1·156	1·033		0·920		0·726	
0·086	1·185	1·082		0·991		0·830	
0·138	1·199	1·117	1·296	1·044		0·911	
0·200	1·208	1·141	1·286	1·080		0·968	
0·269	1·208	1·152	1·269	1·100		1·006	
0·344	1·203	1·157	1·253	1·114		1·032	
0·424	1·183	1·146	1·223	1·110	1·265	1·042	
0·507	1·144	1·115	1·174	1·086	1·204	1·031	1·270
0·592	1·101	1·079	1·124	1·056	1·147	1·012	1·194
0·676	1·061	1·043	1·078	1·026	1·095	0·990	1·129
0·756	1·024	1·011	1·037	0·997	1·050	0·969	1·075
0·829	0·994	0·984	1·004	0·973	1·013	0·951	1·031
0·891	0·967	0·959	0·974	0·951	0·981	0·935	0·993
0·942	0·936	0·931	0·940	0·926	0·945	0·914	0·952
0·978	0·897	0·894	0·900	0·891	0·902	0·884	0·905
0·998	0·824	0·823	0·825	0·822	0·825	0·819	0·825
1·000							

TABLES 3a and 3b

Velocity Distributions

Table 3a

6 per cent RAE 102

$M_\infty = 0$

α	0 deg	1 deg		2 deg		4 deg	
x/c		Upper	Lower	Upper	Lower	Upper	Lower
0							
0·001	0·645	1·074	0·215	1·504		2·361	
0·007	0·984	1·202	0·766	1·420	0·547	1·854	0·109
0·017	1·043	1·181	0·905	1·319	0·766	1·593	0·488
0·033	1·065	1·166	0·965	1·265	0·864	1·464	0·662
0·054	1·073	1·151	0·995	1·228	0·916	1·382	0·759
0·088	1·077	1·136	1·017	1·195	0·957	1·312	0·836
0·143	1·080	1·125	1·034	1·170	0·988	1·315	0·895
0·207	1·081	1·117	1·045	1·153	1·008	1·224	0·934
0·280	1·081	1·110	1·051	1·139	1·021	1·196	0·960
0·359	1·080	1·104	1·055	1·128	1·030	1·176	0·979
0·443	1·071	1·091	1·050	1·111	1·030	1·150	0·987
0·528	1·056	1·073	1·039	1·089	1·022	1·121	0·986
0·614	1·040	1·054	1·026	1·067	1·011	1·093	0·982
0·696	1·024	1·035	1·013	1·046	1·001	1·067	0·976
0·774	1·009	1·018	1·000	1·027	0·990	1·044	0·970
0·843	0·997	1·000	0·990	1·011	0·982	1·024	0·966
0·902	0·986	0·991	0·980	0·996	0·974	1·005	0·962
0·949	0·972	0·975	0·968	0·979	0·964	0·984	0·954
0·981	0·954	0·956	0·951	0·957	0·948	0·960	0·492
0·998	0·916	0·917	0·916	0·917	0·914	0·917	0·911
1·000							

Table 3b

6 per cent RAE 102

$M_\infty = 0{\cdot}70$

α	0 deg	1 deg		2 deg		4 deg	
x/c		Upper	Lower	Upper	Lower	Upper	Lower
0							
0·001	0·645						
0·007	0·978						
0·018	1·063		0·872				
0·033	1·097	1·275	0·950		0·823		
0·054	1·109	1·243	0·991		0·887		
0·088	1·114	1·215	1·022		0·940		0·790
0·141	1·120	1·196	1·048	1·286	0·982		0·862
0·205	1·122	1·182	1·064	1·250	1·010		0·910
0·276	1·121	1·169	1·073	1·222	1·028		0·944
0·354	1·120	1·159	1·080	1·202	1·042	1·300	0·970
0·436	1·106	1·139	1·074	1·174	1·043	1·247	0·983
0·521	1·082	1·110	1·057	1·136	1·032	1·192	0·982
0·606	1·058	1·080	1·038	1·101	1·017	1·143	0·976
0·690	1·034	1·052	1·019	1·069	1·002	1·101	0·968
0·768	1·013	1·027	1·001	1·039	0·987	1·064	0·960
0·839	0·996	1·006	0·986	1·016	0·976	1·034	0·954
0·899	0·980	0·987	0·972	0·994	0·964	1·007	0·948
0·947	0·961	0·966	0·956	0·970	0·950	0·978	0·938
0·980	0·937	0·939	0·933	0·942	0·930	0·945	0·922
0·998	0·889	0·889	0·887	0·889	0·886	0·889	0·882
1·000							

TABLES 3c and 4a

Velocity Distributions

Table 3c

6 per cent RAE 102

$M_\infty = 0{\cdot}80$

α	0 deg	1 deg		2 deg		4 deg	
x/c		Upper	Lower	Upper	Lower	Upper	Lower
0							
0·001	0·645						
0·007	0·975						
0·018	1·071		0·853				
0·034	1·115		0·939		0·860		
0·054	1·133		0·987		0·923		
0·088	1·144		1·025		0·972		
0·141	1·152		1·056		1·008		0·843
0·203	1·157		1·078		1·034		0·896
0·274	1·156		1·090		1·051		0·934
0·351	1·154		1·099		1·065		0·964
0·432	1·138	1·191	1·094		1·066		0·980
0·515	1·106	1·143	1·072	1·186	1·049		0·979
0·601	1·074	1·101	1·047	1·130	1·030	1·197	0·972
0·684	1·044	1·065	1·023	1·086	1·010	1·130	0·963
0·763	1·017	1·033	1·002	1·049	0·992	1·080	0·954
0·835	0·996	1·008	0·984	1·019	0·977	1·042	0·946
0·896	0·977	0·985	0·968	0·993	0·964	1·008	0·939
0·945	0·954	0·960	0·948	0·965	0·946	0·974	0·928
0·980	0·926	0·929	0·922	0·932	0·923	0·936	0·910
0·998	0·872	0·873	0·871	0·873	0·871	0·873	0·865
1·000							

Table 4a

6 per cent RAE 104

$M_\infty = 0$

α	0 deg	1 deg		2 deg		4 deg	
x/c		Upper	Lower	Upper	Lower	Upper	Lower
0							
0·001	0·659	1·098	0·220	1·537		2·412	
0·007	0·973	1·189	0·757	1·404	0·541	1·833	0·108
0·018	1·024	1·159	0·888	1·295	1·752	1·564	0·479
0·034	1·046	1·145	0·948	1·243	0·849	1·438	0·650
0·054	1·057	1·134	0·980	1·210	0·903	1·362	0·748
0·090	1·063	1·122	1·004	1·180	0·945	1·296	0·825
0·145	1·067	1·112	1·022	1·156	0·976	1·300	0·885
0·210	1·069	1·104	1·033	1·140	0·996	1·209	0·423
0·284	1·069	1·098	1·040	1·127	1·010	1·183	0·949
0·363	1·069	1·094	1·045	1·117	1·020	1·164	0·970
0·447	1·069	1·089	1·048	1·109	1·027	1·147	0·985
0·533	1·068	1·084	1·050	1·101	1·033	1·133	0·997
0·617	1·060	1·074	1·046	1·088	1·031	1·114	1·001
0·698	1·040	1·051	1·028	1·062	1·016	1·084	0·991
0·774	1·019	1·028	1·009	1·037	1·000	1·053	0·979
0·843	1·001	1·008	0·994	1·015	0·986	1·028	0·970
0·902	0·986	0·991	0·980	0·996	0·974	1·005	0·962
0·948	0·969	0·972	0·965	0·976	0·960	0·981	0·951
0·981	0·946	0·948	0·944	0·950	0·942	0·953	0·935
0·998	0·902	0·903	0·902	0·903	0·901	0·903	0·898
1·000							

TABLES 4b and 4c

Velocity Distributions

	α	0 deg	1 deg		2 deg		4 deg	
	x/c		Upper	Lower	Upper	Lower	Upper	Lower
	0							
Table 4b	0·001	0·659	1·171					
	0·007	0·969						
6 per cent RAE 104	0·018	1·036	1·268	0·855				
	0·034	1·068	1·235	0·929		0·806		
$M_\infty = 0{\cdot}70$	0·055	1·084	1·214	0·973		0·872		
	0·090	1·093	1·191	1·005		0·925		0·779
	0·144	1·098	1·173	1·030	1·258	0·967		0·850
	0·209	1·101	1·160	1·046	1·224	0·994		0·897
	0·281	1·102	1·149	1·057	1·200	1·013		0·931
	0·360	1·102	1·142	1·065	1·183	1·028	1·275	0·958
	0·443	1·101	1·134	1·070	1·168	1·038	1·240	0·978
	0·528	1·100	1·127	1·073	1·155	1·047	1·212	0·995
	0·611	1·090	1·112	1·068	1·134	1·046	1·180	1·002
	0·692	1·060	1·077	1·042	0·194	1·025	1·128	0·989
	0·769	1·028	1·041	1·014	1·054	1·001	1·079	0·973
	0·839	1·002	1·012	0·992	1·022	0·981	1·040	0·959
	0·899	0·981	0·988	0·973	0·995	0·965	1·008	0·948
	0·946	0·957	0·962	0·952	0·966	0·946	0·974	0·934
	0·980	0·927	0·930	0·924	0·932	0·921	0·936	0·913
	0·998	0·871	0·871	0·870	0·872	0·868	0·871	0·864
	1·000							
	0							
Table 4c	0·001	0·659						
	0·007	0·954						
6 per cent RAE 104	0·018	1·039		0·834				
	0·035	1·080		0·916				
$M_\infty = 0{\cdot}80$	0·056	1·102		0·965		0·853		
	0·090	1·114		1·004		0·912		
	0·144	1·124		1·035		0·960		0·829
	0·208	1·127		1·055		0·992		0·881
	0·281	1·129		1·068		1·014		0·919
	0·359	1·130	1·189	1·079		1·032		0·950
	0·441	1·128	1·178	1·085		1·046		0·974
	0·524	1·126	1·167	1·090		1·056		0·993
	0·607	1·114	1·146	1·085	1·181	1·056		1·003
	0·688	1·075	1·098	1·053	1·121	1·031	1·172	0·988
	0·765	1·035	1·051	1·019	1·008	1·002	1·101	0·969
	0·835	1·003	1·015	0·991	1·027	0·978	1·049	0·953
	0·896	0·977	0·986	0·968	0·994	0·959	1·009	0·940
	0·945	0·950	0·955	0·944	0·960	0·937	0·969	0·923
	0·979	0·916	0·919	0·912	0·921	0·909	0·925	0·900
	0·998	0·853	0·854	0·852	0·854	0·850	0·854	0·846
	1·000							

TABLES 5a and 5b

Velocity Distributions

	α	0 deg	1 deg		2 deg		4 deg	
	x/c		Upper	Lower	Upper	Lower	Upper	Lower
	0							
Table 5a	0·001	0·764	1·272	0·254	1·781		2·796	
	0·007	0·997	1·218	0·776	1·438	0·554	1·878	0·111
4 per cent RAE 104	0·018	1·027	1·163	0·891	1·299	0·754	1·569	0·480
	0·034	1·036	1·134	0·938	1·231	0·840	1·424	0·644
$M_\infty = 0$	0·055	1·041	1·117	0·965	1·192	0·889	1·341	0·736
	0·090	1·044	1·102	0·986	1·159	0·928	1·272	0·810
	0·145	1·046	1·090	1·002	1·133	0·957	1·274	0·867
	0·211	1·047	1·081	1·011	1·116	0·976	1·185	0·904
	0·285	1·047	1·075	1·018	1·103	0·988	1·159	0·929
	0·366	1·047	1·070	1·023	1·094	0·998	1·140	0·949
	0·450	1·046	1·066	1·026	1·086	1·006	1·124	0·964
	0·536	1·046	1·062	1·029	1·079	1·012	1·110	0·976
	0·621	1·042	1·055	1·028	1·069	1·013	1·095	0·983
	0·702	1·027	1·038	1·016	1·049	1·040	1·070	0·979
	0·778	1·013	1·022	1·004	1·031	0·994	1·047	0·974
	0·846	1·001	1·008	0·994	1·015	0·986	1·027	0·970
	0·904	0·990	0·996	0·985	1·001	0·979	1·010	0·966
	0·950	0·978	0·982	0·975	0·985	0·970	0·991	0·961
	0·982	0·963	0·965	0·961	0·967	0·958	0·970	0·952
	0·998	0·932	0·932	0·931	0·933	0·970	0·933	0·927
	1·000							
	0							
Table 5b	0·001	0·764						
	0·007	1·002		0·727				
4 per cent RAE 104	0·018	1·041	1·277	0·859				
	0·034	1·053	1·214	0·918		0·797		
$M_\infty = 0{\cdot}70$	0·055	1·060	1·183	0·953		0·856		
	0·090	1·065	1·157	0·981	1·265	0·904		0·763
	0·145	1·069	1·138	1·004	1·216	0·943		0·830
	0·210	1·069	1·124	1·017	1·183	0·968		0·874
	0·284	1·069	1·161	1·026	1·160	0·985	1·265	0·906
	0·364	1·069	1·105	1·133	1·144	0·999	1·226	0·932
	0·447	1·068	1·099	1·038	1·130	1·009	1·196	0·952
	0·533	1·068	1·093	1·042	1·119	1·018	1·172	0·968
	0·616	1·063	1·084	1·042	1·105	1·021	1·147	0·979
	0·698	1·040	1·057	1·023	1·074	1·006	1·106	0·972
	0·774	1·019	1·032	1·006	1·045	0·992	1·070	0·965
	0·843	1·002	1·012	0·991	1·021	0·981	1·039	0·959
	0·902	0·986	0·994	0·979	1·001	0·971	1·014	0·954
	0·948	0·970	0·975	0·964	0·979	0·959	0·987	0·946
	0·981	0·949	0·951	0·946	0·954	0·942	0·957	0·934
	0·998	0·907	0·908	0·906	0·908	0·905	0·908	0·901
	1·000							

TABLES 5c and 5d

Velocity Distributions

Table 5c

4 per cent RAE 104

$M_\infty = 0{\cdot}80$

α	0 deg	1 deg		2 deg		4 deg	
x/c		Upper	Lower	Upper	Lower	Upper	Lower
0							
0·001	0·764						
0·007	0·997						
0·018	1·047		0·839				
0·034	1·063		0·904				
0·055	1·073		0·944		0·836		
0·090	1·078		0·976		0·889		
0·144	1·082	1·182	1·002		0·932		0·807
0·209	1·084	1·160	1·019		0·960		0·856
0·283	1·084	1·145	1·030		0·981		0·892
0·362	1·084	1·134	1·039	1·195	0·997		0·920
0·446	1·084	1·125	1·046	1·172	1·010		0·943
0·530	1·084	1·118	1·051	1·155	1·021		0·963
0·614	1·078	1·105	1·051	1·135	1·025		0·975
0·695	1·049	1·071	1·029	1·092	1·008	1·137	0·968
0·772	1·024	1·040	1·008	1·056	0·992	1·088	0·959
0·844	1·002	1·014	0·990	1·026	0·977	1·048	0·952
0·900	0·984	0·993	0·975	1·001	0·966	1·017	0·946
0·948	0·965	0·970	0·958	0·976	0·952	0·985	0·938
0·980	0·940	0·943	0·937	0·946	0·933	0·950	0·924
0·998	0·894	0·894	0·892	0·895	0·891	0·894	0·886
1·000							

Table 5d

4 per cent RAE 104

$M_\infty = 0{\cdot}85$

α	0 deg	1 deg		2 deg		4 deg	
x/c		Upper	Lower	Upper	Lower	Upper	Lower
0							
0·001	0·764						
0·007	0·994						
0·018	1·054		0·824				
0·034	1·074		0·894				
0·055	1·086		0·937		0·821		
0·090	1·094		0·973		0·878		
0·144	1·099		1·002		0·924		
0·209	1·101		1·022		0·955		0·843
0·282	1·102		1·036		0·979		0·881
0·361	1·103		1·046		0·998		0·912
0·444	1·103		1·054		1·012		0·937
0·528	1·040		1·063		1·026		0·960
0·611	1·099	1·140	1·065		1·033		0·976
0·692	1·061	1·098	1·036	1·117	1·012		0·966
0·769	1·029	1·048	1·010	1·067	0·991	1·108	0·955
0·839	1·003	1·017	0·989	1·030	0·975	1·057	0·946
0·899	0·982	0·992	0·972	1·001	0·961	1·019	0·940
0·946	0·960	0·966	0·953	0·972	0·946	0·982	0·930
0·980	0·932	0·935	0·928	0·938	0·924	0·943	0·914
0·998	0·881	0·882	0·879	0·882	0·878	0·882	0·873
1·000							

TABLE 6

Aerofoil	M_{∞}	$\partial C_L / \partial \alpha$	$-\partial C_m / \partial \alpha$	h
10 per cent RAE 102	0 0·70	6·72 10·94	1·75 2·80	0·260 0·256
6 per cent RAE 102	0 0·70 0·80	6·59 9·98 13·77	1·69 2·52 3·40	0·256 0·252 0·247
10 per cent RAE 104*	0 0·70	6·78 10·89	1·80 2·86	0·266 0·263
6 per cent RAE 104	0 0·70 0·80	6·56 9·82 13·05	1·70 2·54 3·39	0·259 0·259 0·260
4 per cent RAE 104	0 0·70 0·80	6·49 9·52 12·02	1·66 2·42 3·06	0·256 0·254 0·255

Pitching moments about leading edge.

TABLE 7

Aerofoil	M_{crit}
10 per cent RAE 102	0·782
6 per cent RAE 102	0·838
10 per cent RAE 104	0·794
6 per cent RAE 104	0·853
4 per cent RAE 104	0·885

Critical Mach number estimated from $C_{p\,0\,min}$ by the Kármán-Tsien Rule

* The results for this aerofoil are taken from Ref. 2.

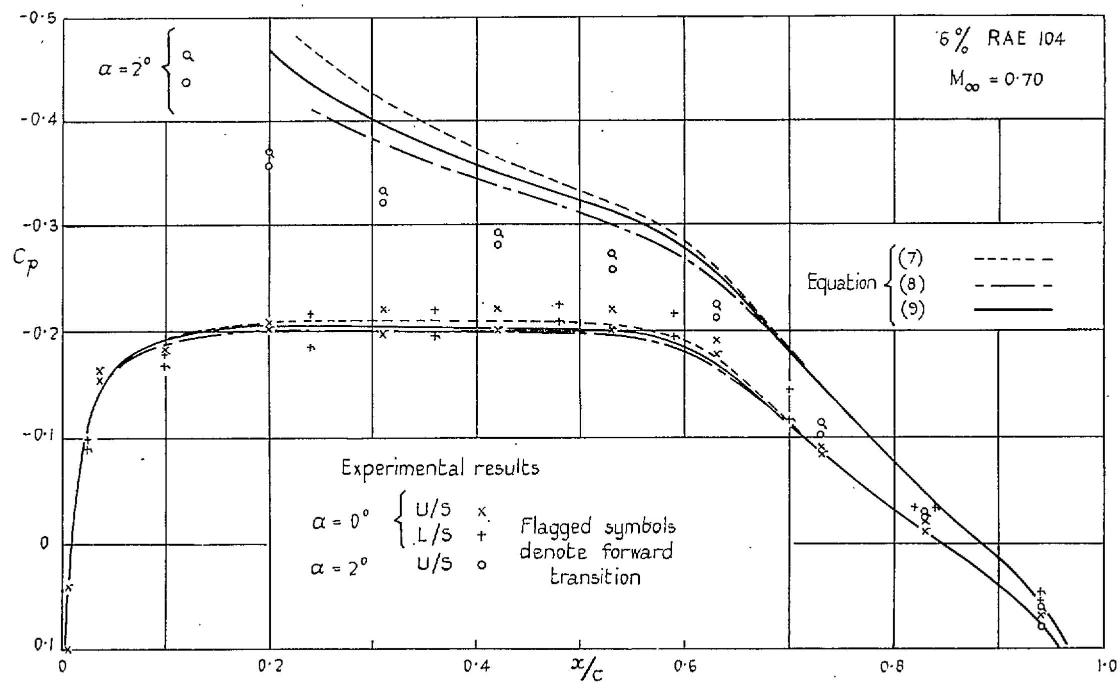

FIG. 1. Comparison between definitions of r and experiment.

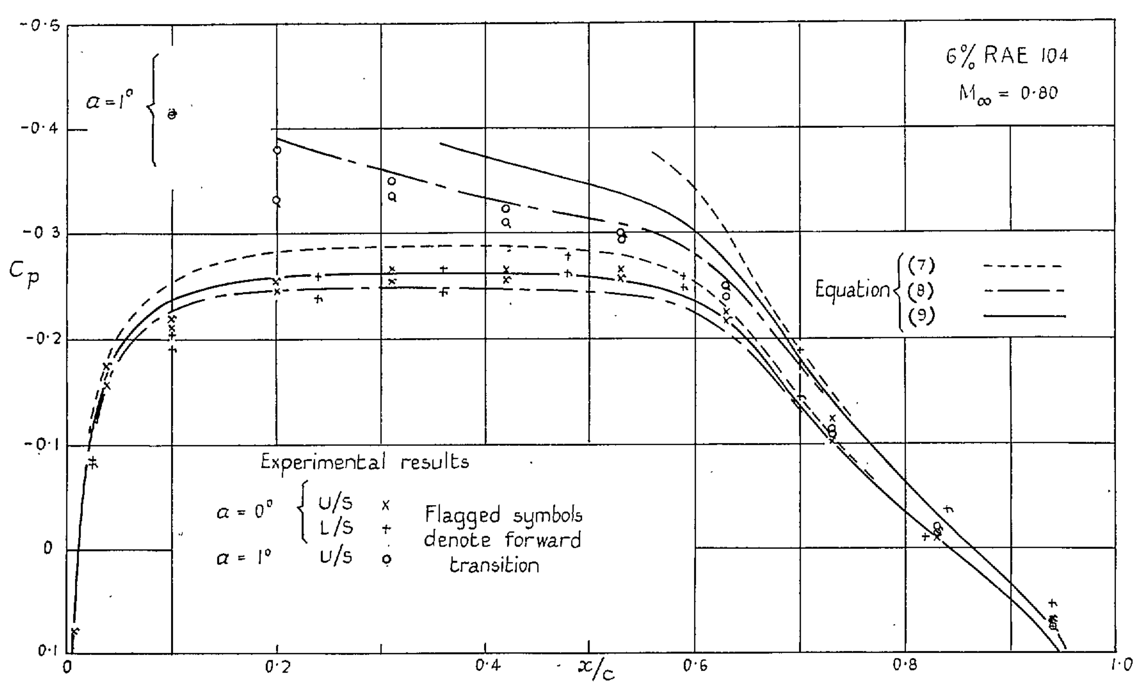

FIG. 2. Comparison between definitions of r and experiment.

FIGS. 3 to 14 show the results given in Tables 2 to 5 plotted in terms of C_p or p/p_0.

A scale of local Mach number is given on the right-hand side of those Figures showing compressible-flow pressure distributions.

The aerofoil and free-stream Mach number are indicated in the top right-hand corner of each Figure.

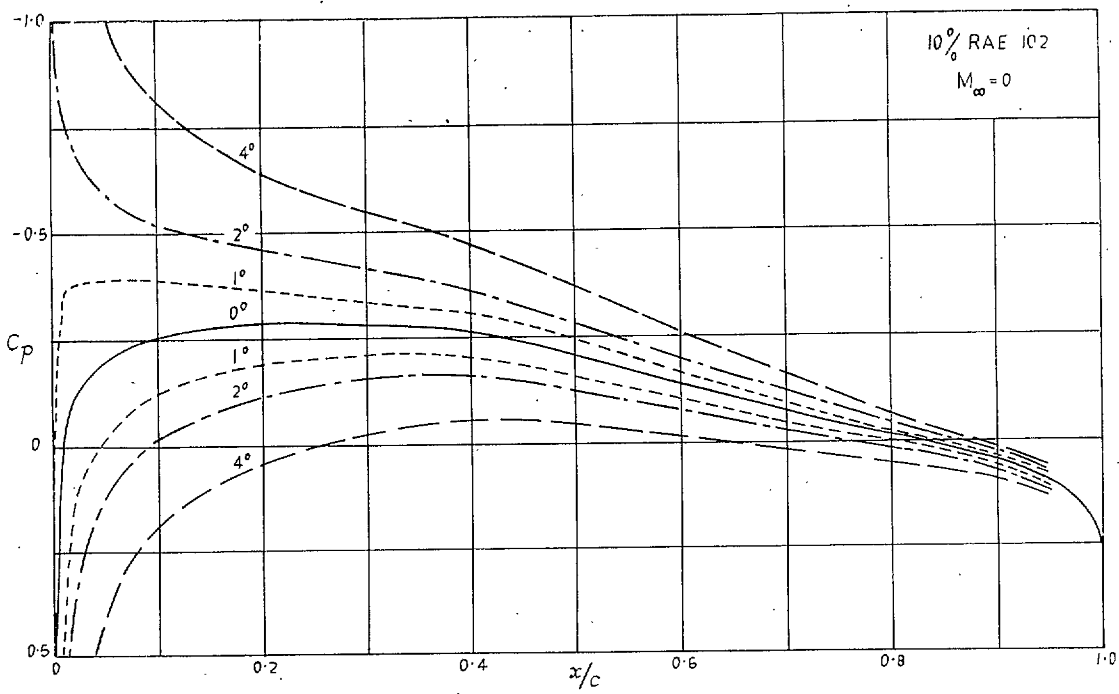

FIG. 3. Variation of C_p with x/c for $\alpha = 0, 1, 2$ and 4 deg.

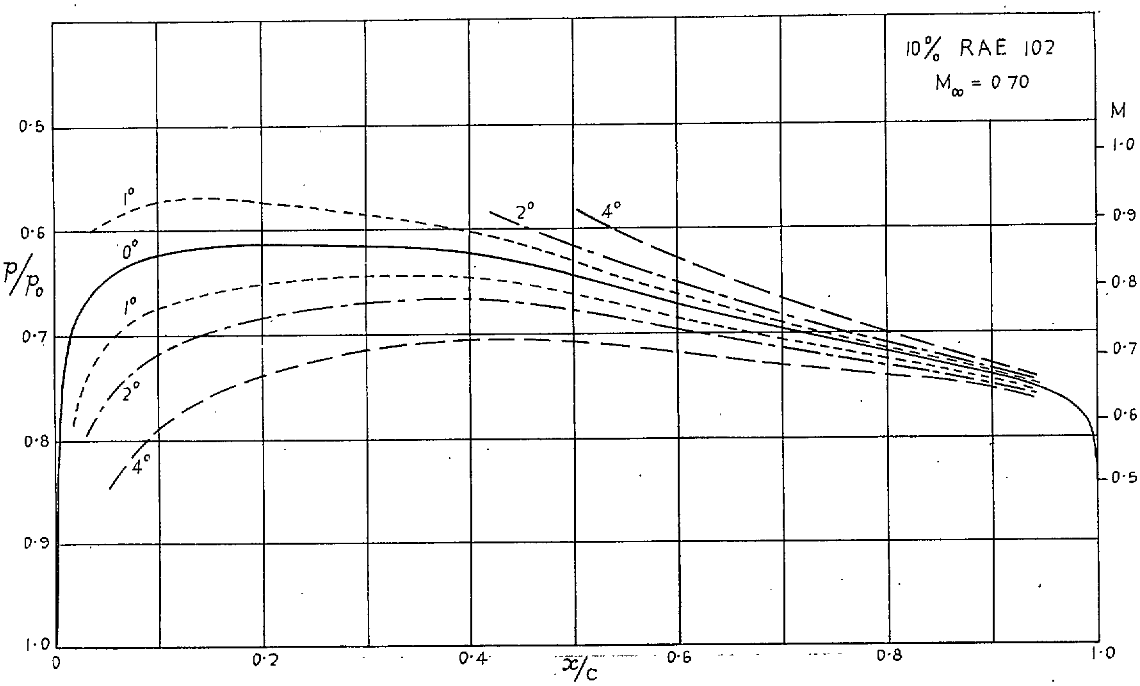

FIG. 4. Variation of p/p_0 with x/c for $\alpha = 0, 1, 2$ and 4 deg.

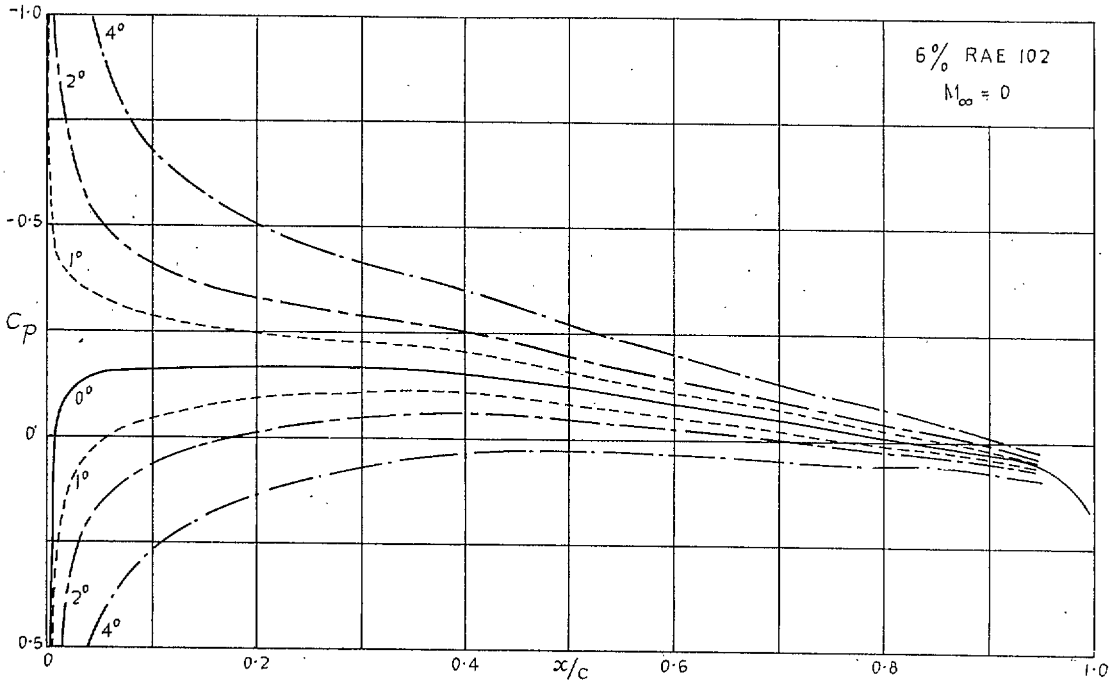

FIG. 5. Variation of C_p with x/c for $\alpha = 0$, 1, 2 and 4 deg.

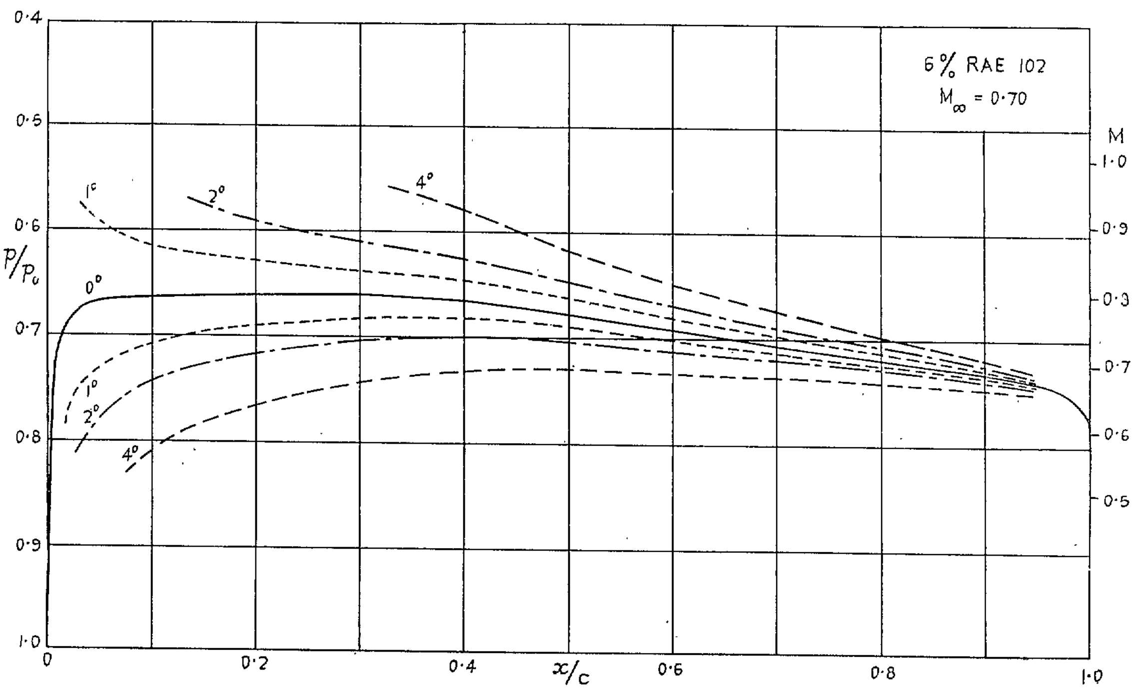

FIG. 6. Variation of p/p_0 with x/c for $\alpha = 0$, 1, 2 and 4 deg.

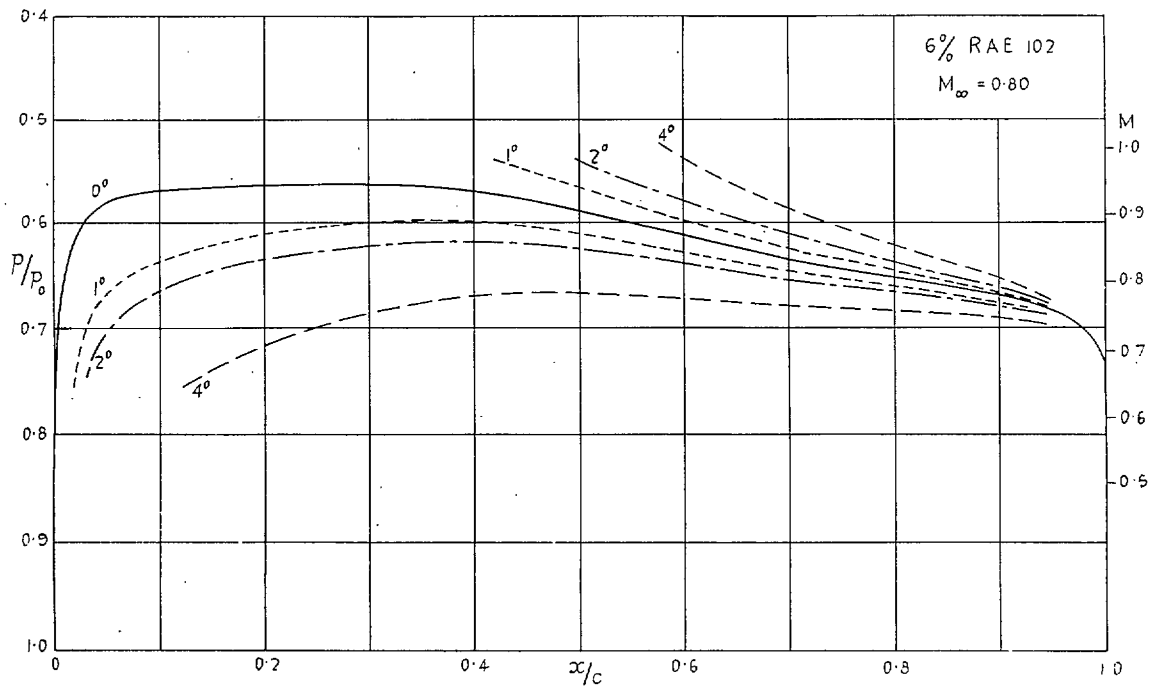

FIG. 7. Variation of p/p_0 with x/c for $\alpha = 0$, 1, 2 and 4 deg.

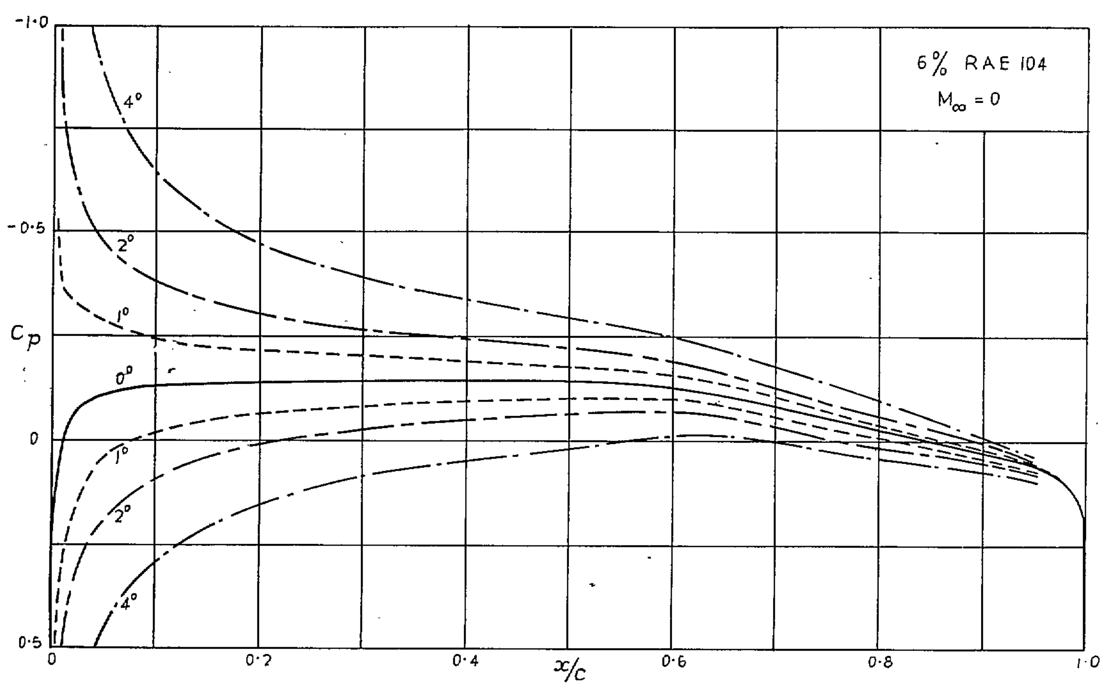

FIG. 8. Variation of C_p with x/c for $\alpha = 0$, 1, 2 and 4 deg.

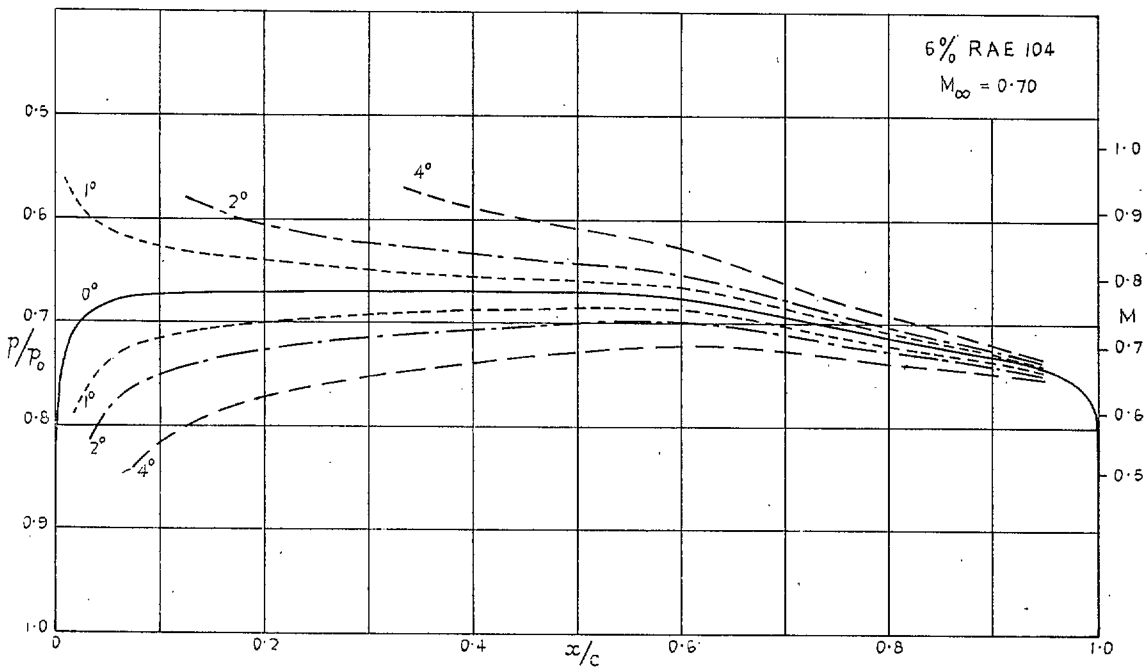

FIG. 9. Variation of p/p_0 with x/c for $\alpha = 0, 1, 2$ and 4 deg.

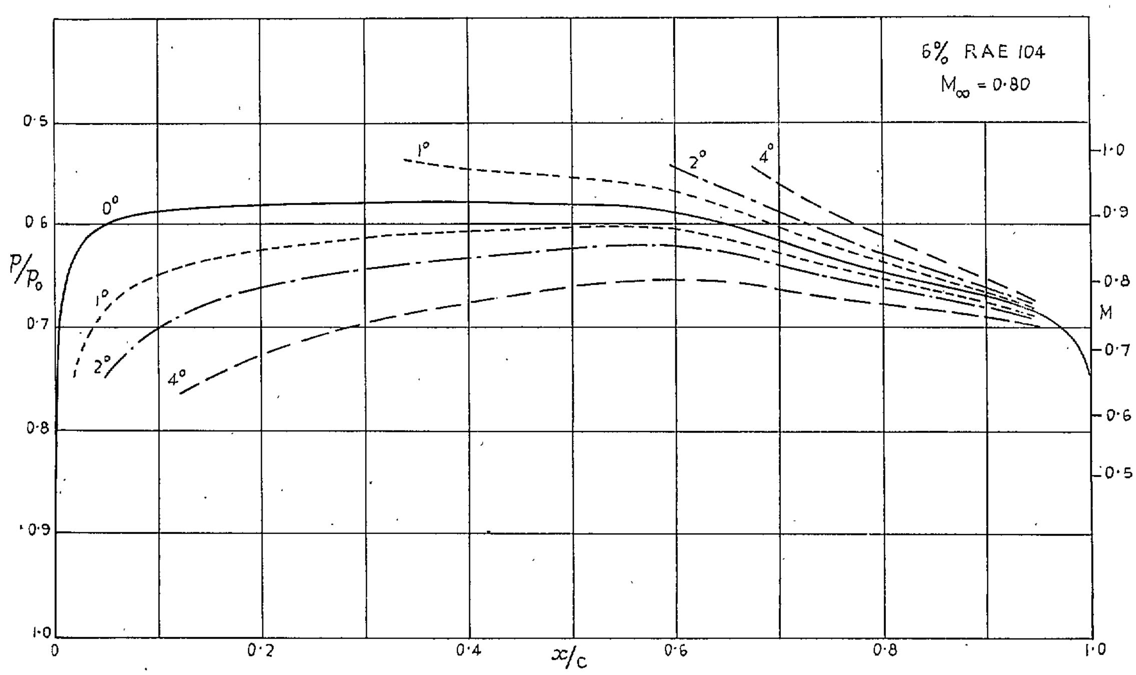

FIG. 10. Variation of p/p_0 with x/c for $\alpha = 0, 1, 2$ and 4 deg.

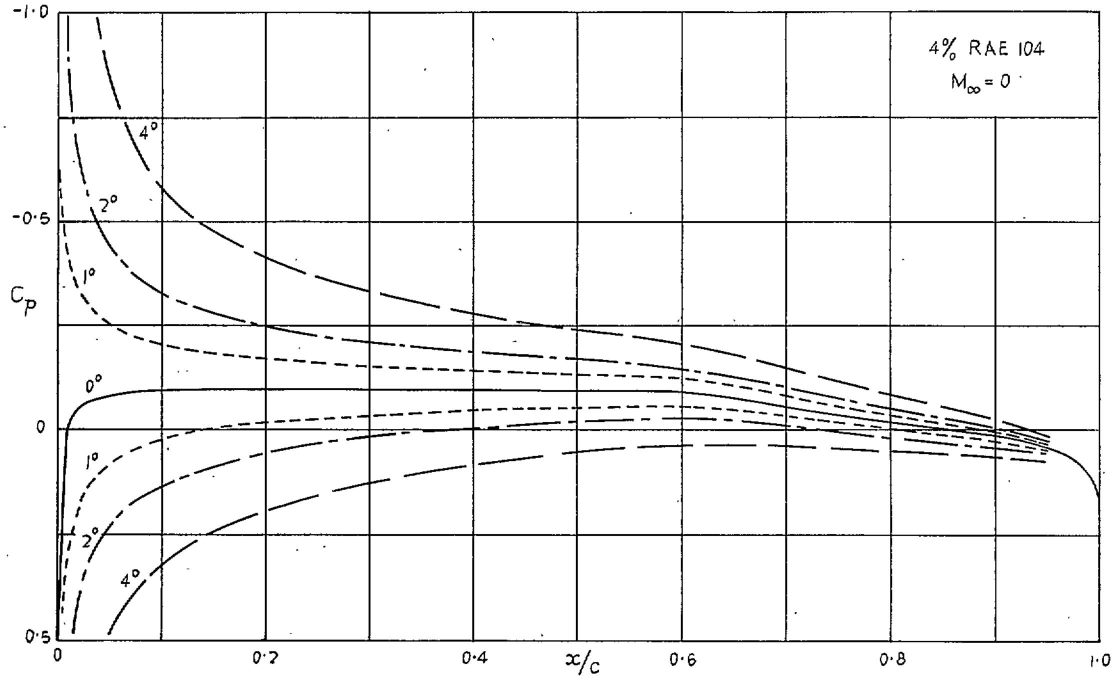

FIG. 11. Variation of C_p with x/c for $\alpha = 0$, 1, 2 and 4 deg.

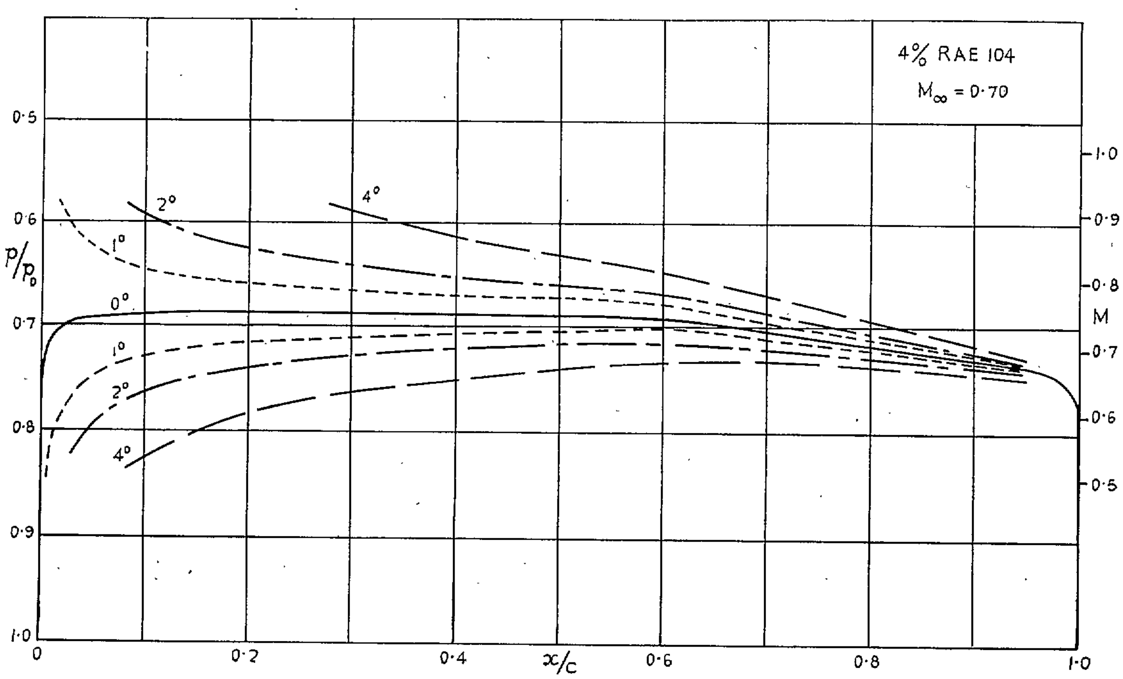

FIG. 12. Variation of p/p_0 with x/c for $\alpha = 0$, 1, 2 and 4 deg.

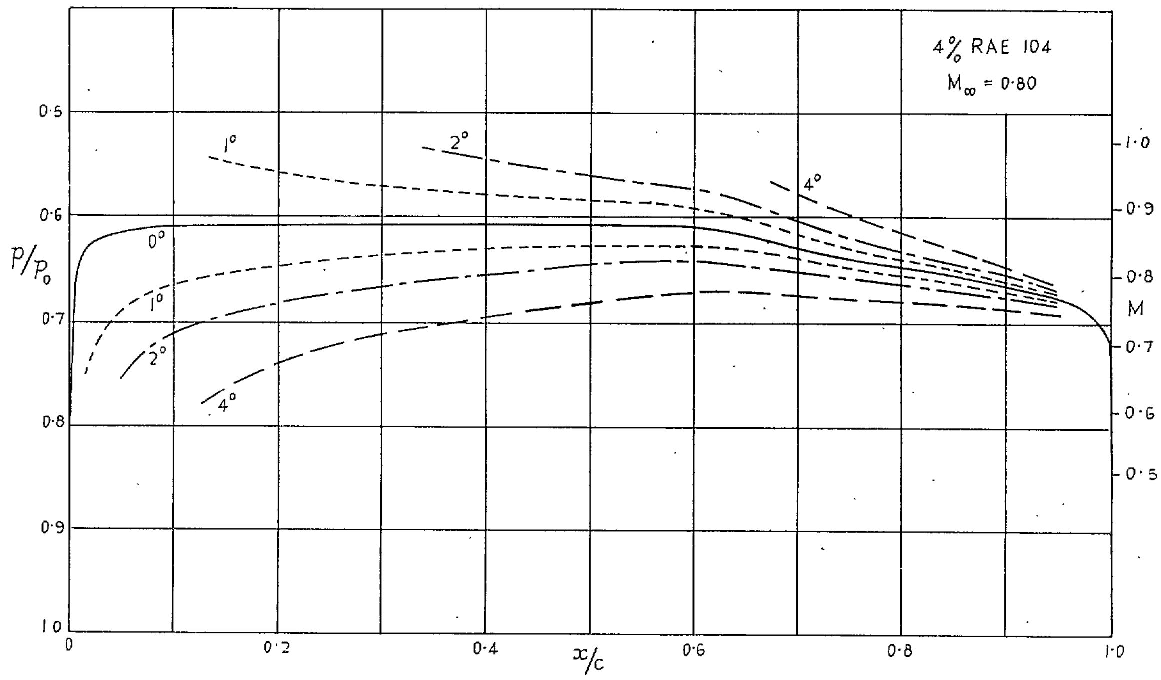

FIG. 13. Variation of p/p_0 with x/c for $\alpha = 0$, 1, 2 and 4 deg.

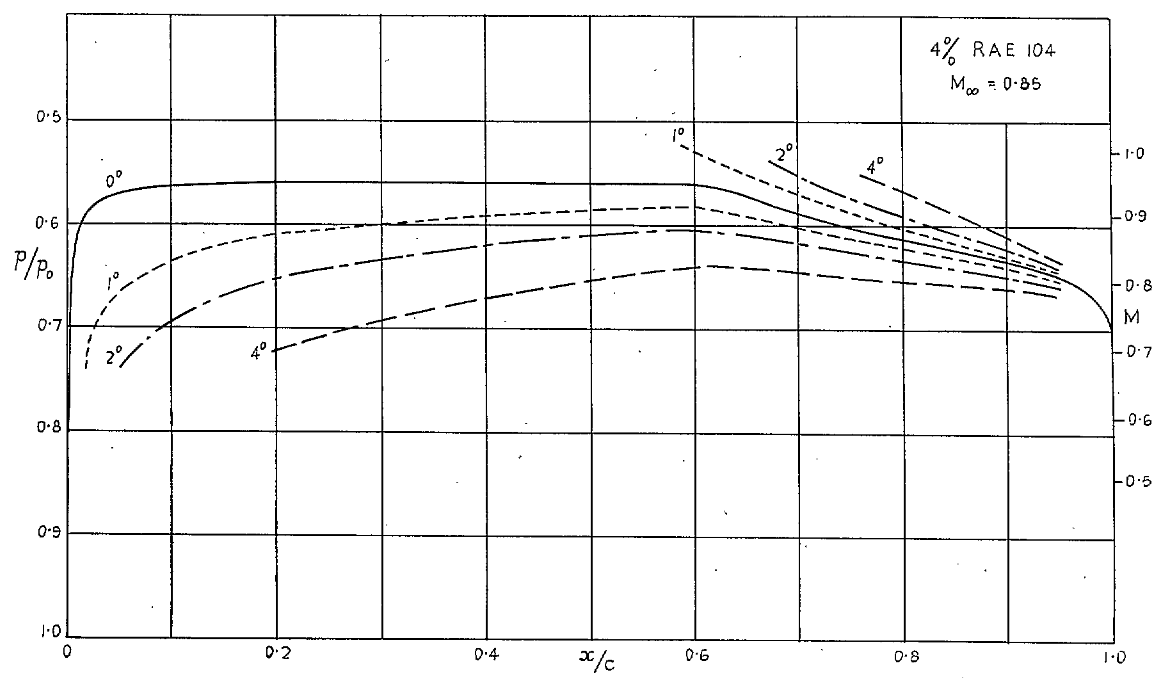

FIG. 14. Variation of p/p_0 with x/c for $\alpha = 0$, 1, 2 and 4 deg.

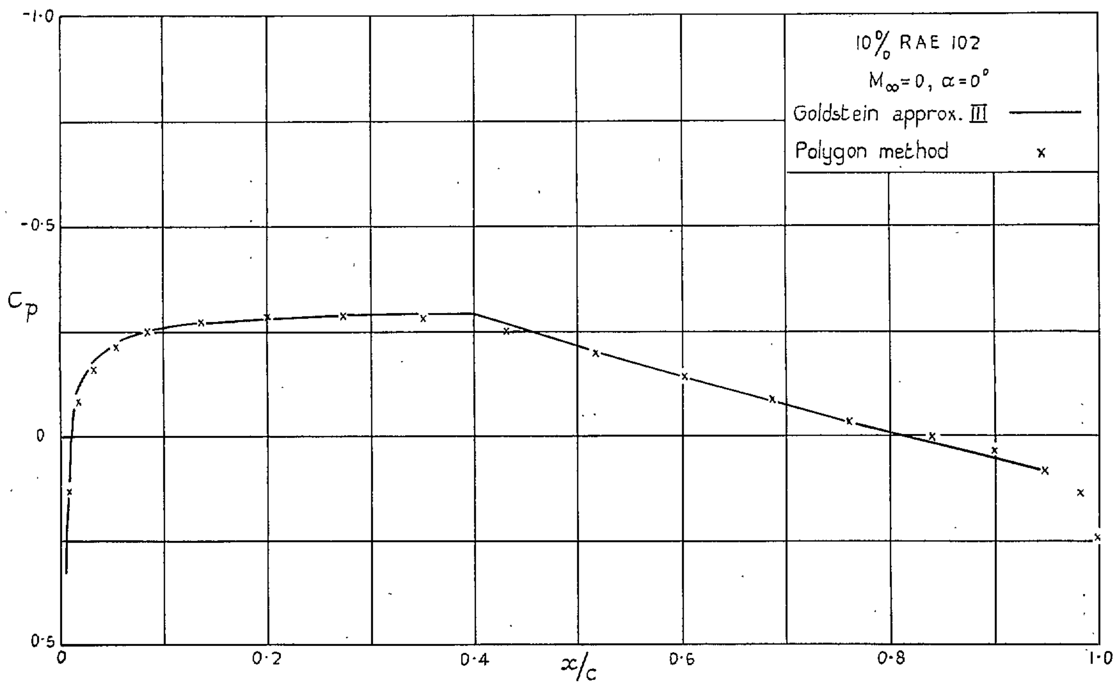

FIG. 15. The effect of the singularity in aerofoil curvature at $x = 0 \cdot 4c$.

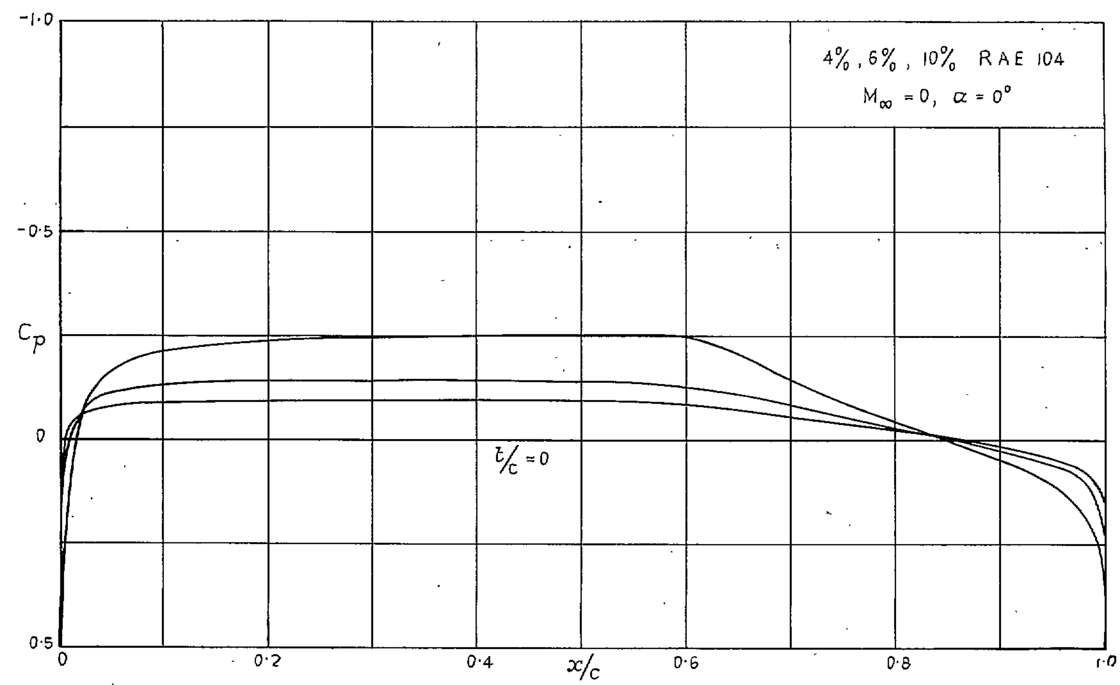

FIG. 16. Effect of thickness at low speed.

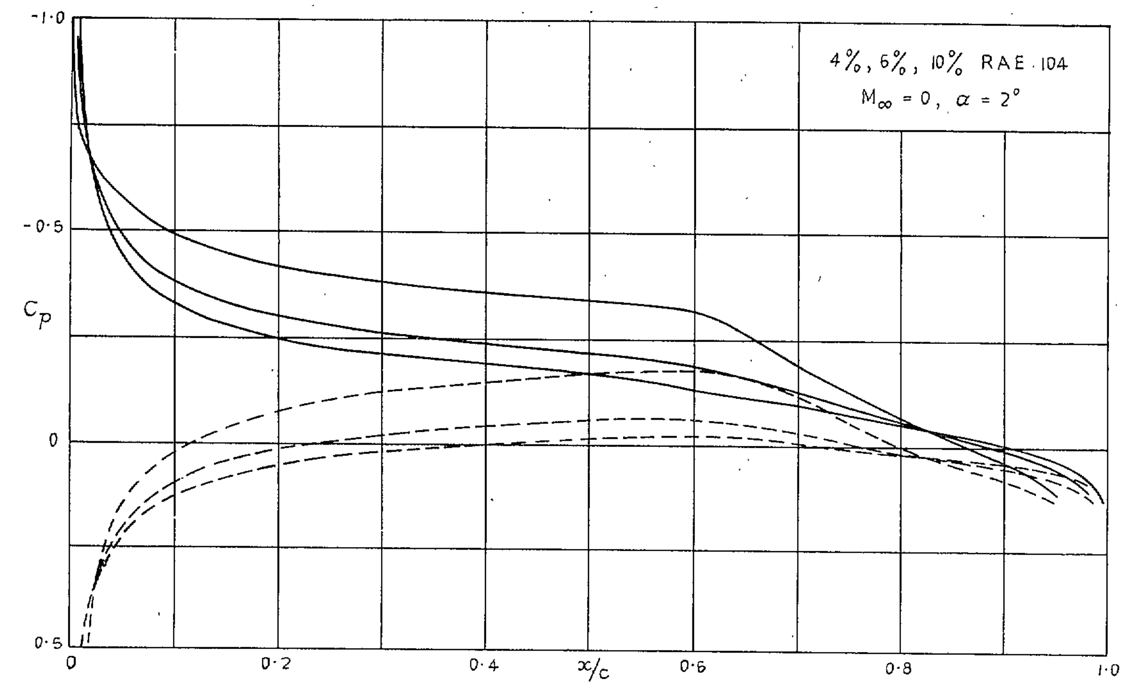

FIG. 17. Effect of thickness at low speed.

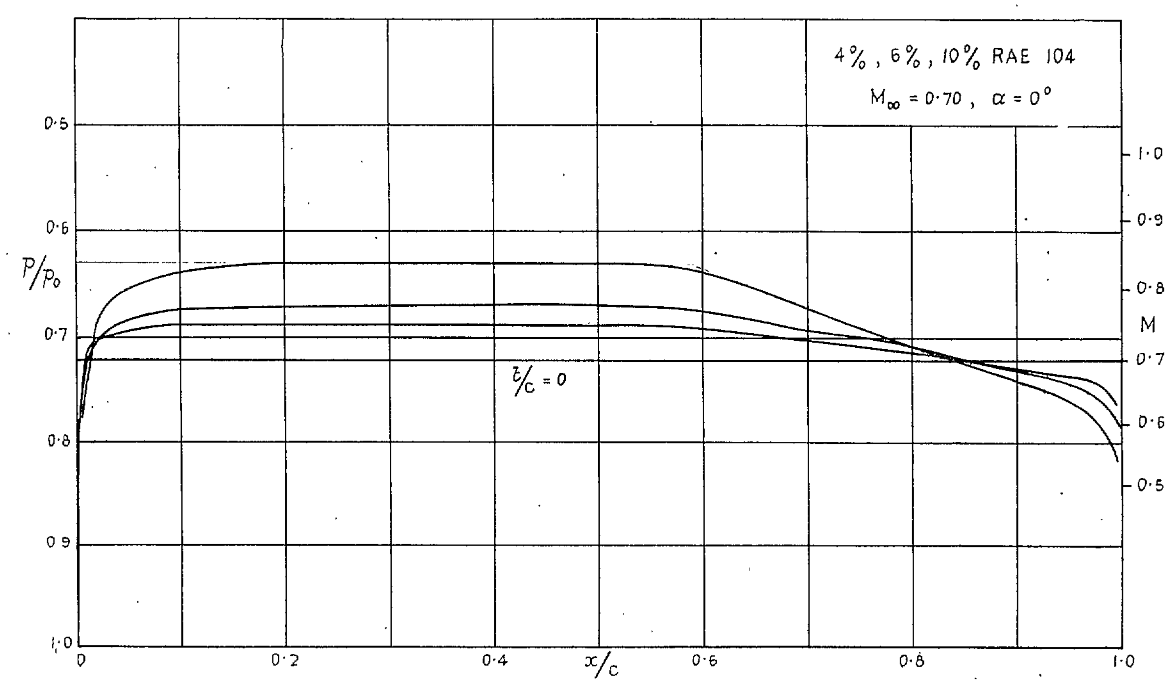

FIG. 18. Effect of thickness at high speed.

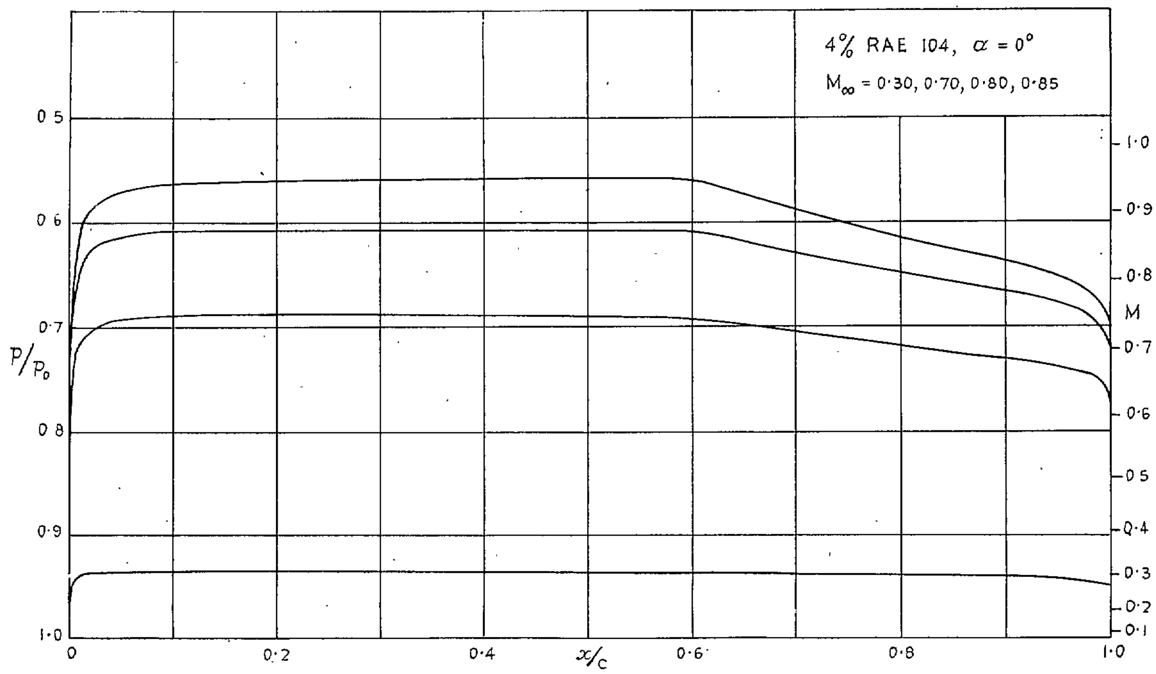

FIG. 19. Variation of chordwise pressure distribution with Mach number.

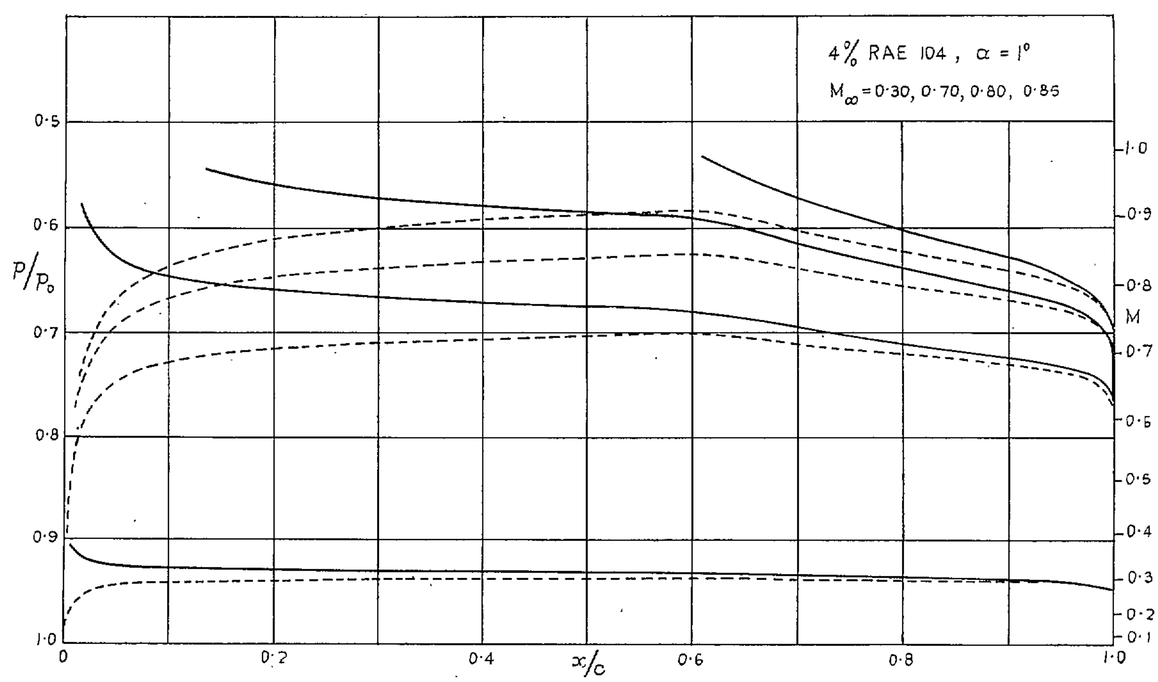

FIG. 20. Variation of chordwise pressure distribution with Mach number.

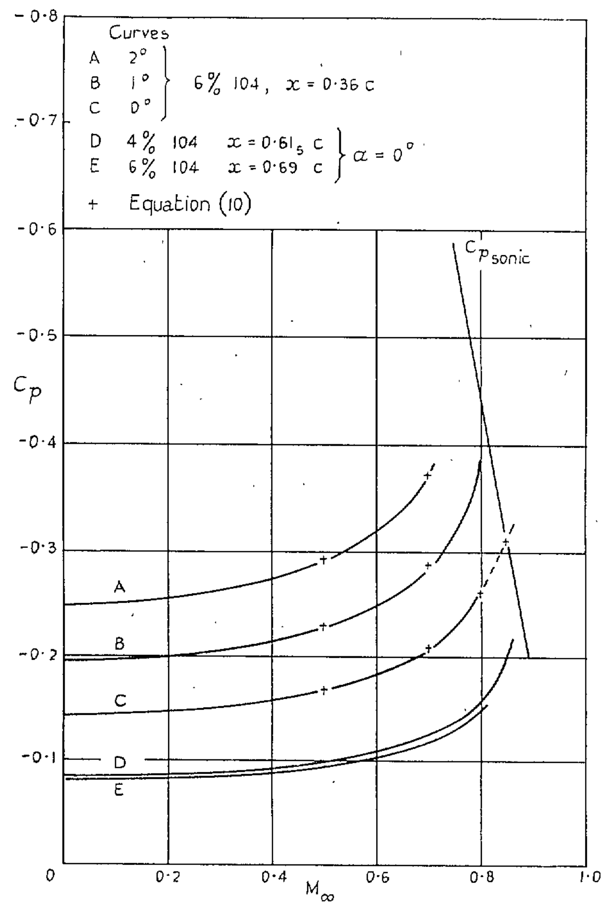

FIG. 21. Variation of C_p with Mach number.

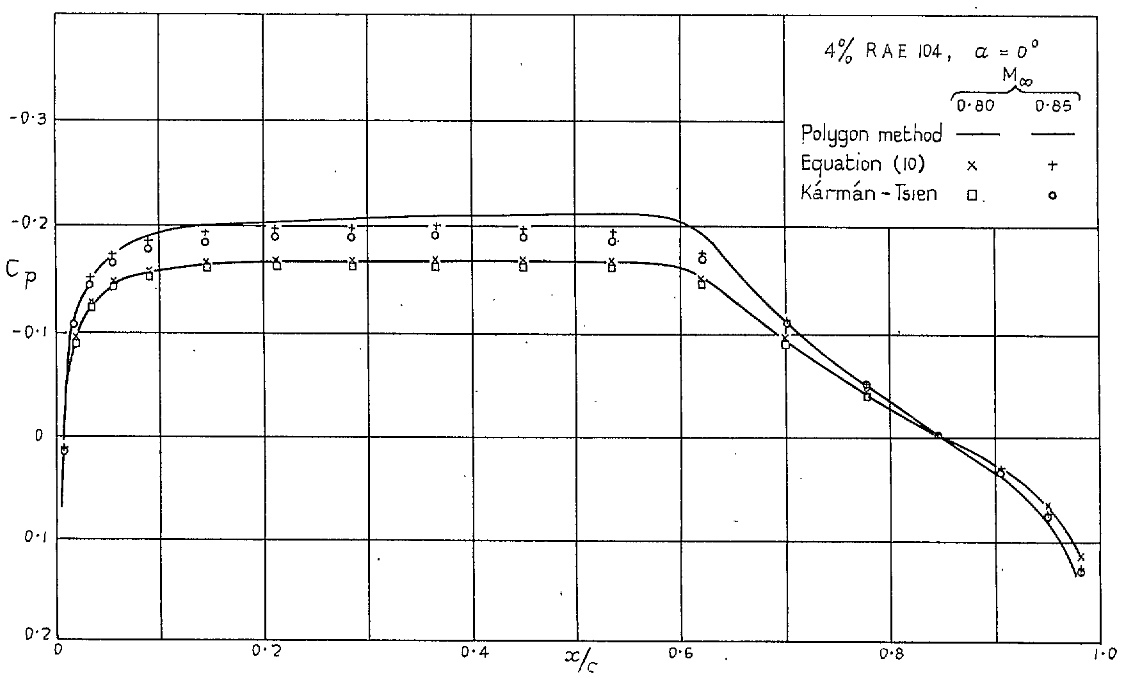

FIG. 22. Comparison between Polygon method and approximate formulae.

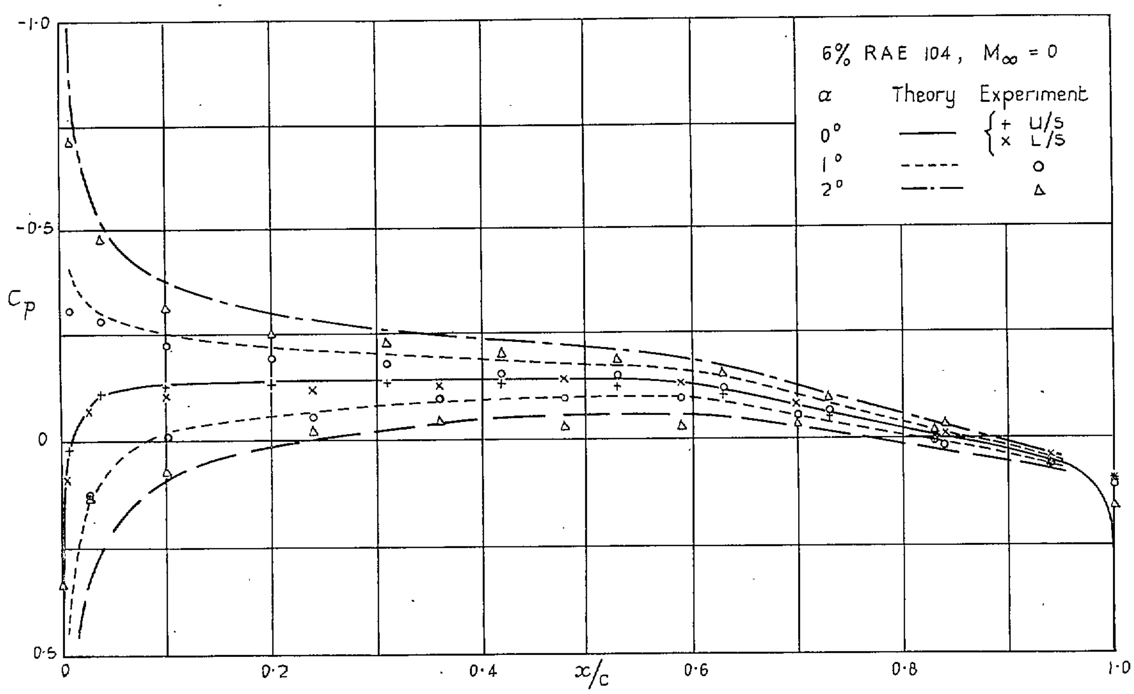

FIG. 23. Comparison with experiment.

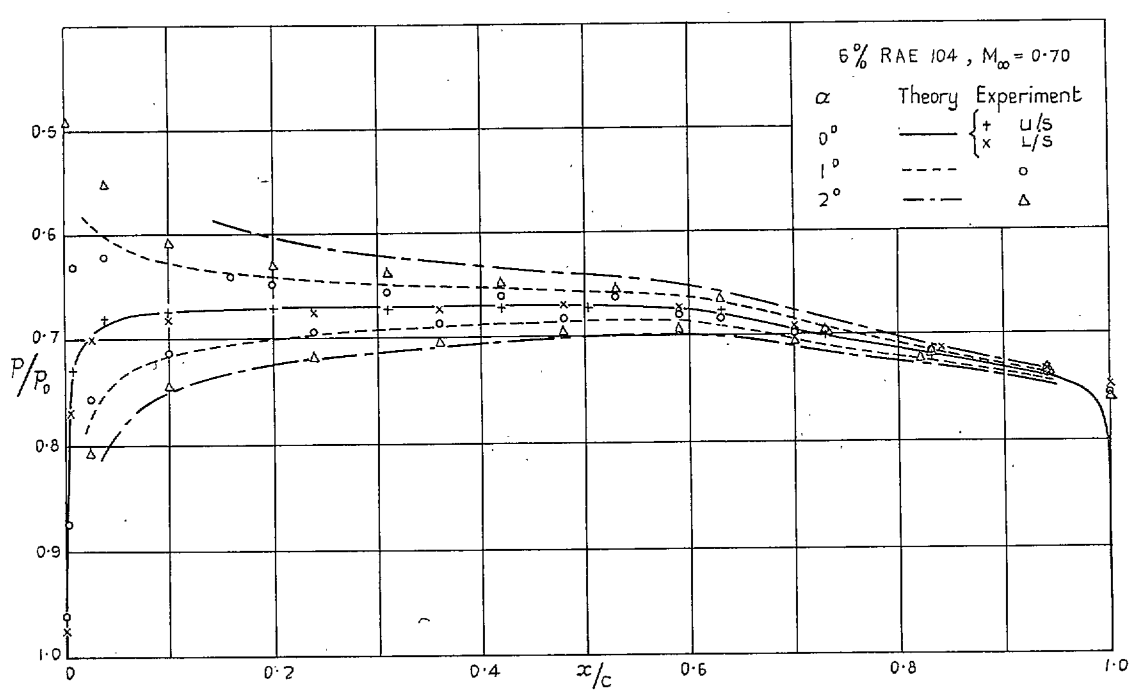

FIG. 24. Comparison with experiment.

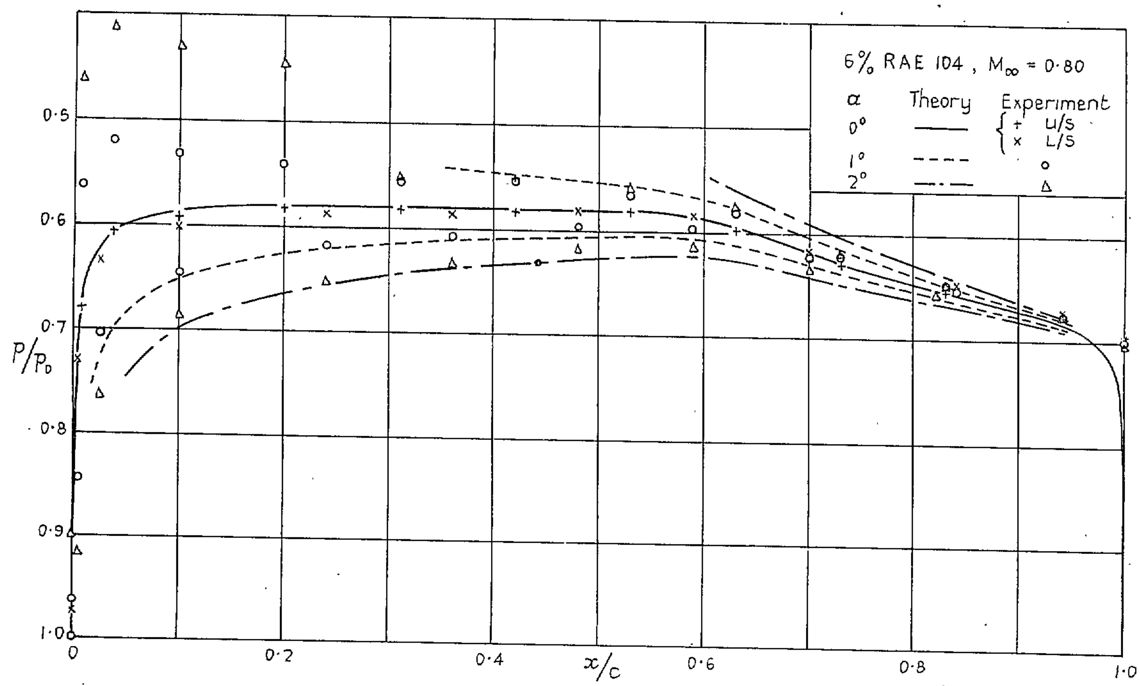

FIG. 25. Comparison with experiment.

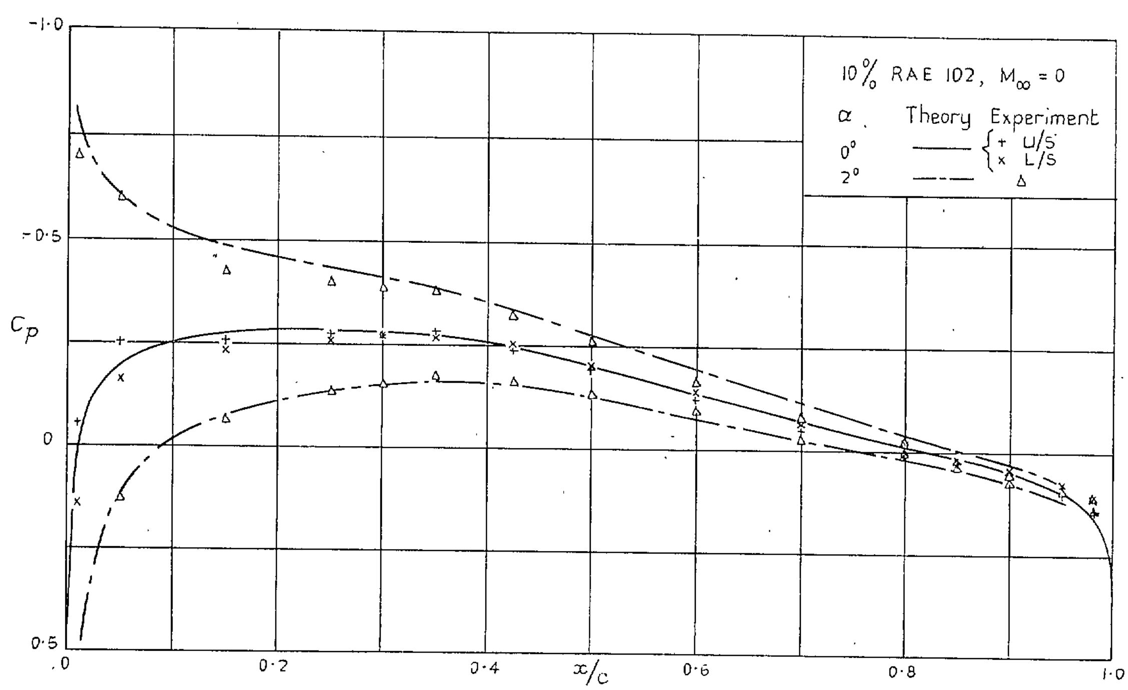

FIG. 26. Comparison with experiment.

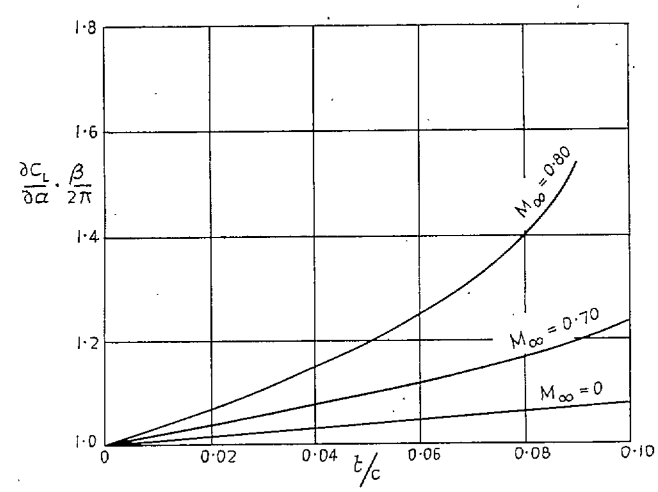

FIG. 27. Thickness and Mach number effect on lift slopes for the RAE 104 aerofoils.

Publication of the Aeronautical Research Council

ANNUAL TECHNICAL REPORTS OF THE AERONAUTICAL RESEARCH COUNCIL (BOUND VOLUMES)

1939 Vol. I. Aerodynamics General, Performance, Airscrews, Engines. 50*s.* (51*s.* 9*d.*).
Vol. II. Stability and Control, Flutter and Vibration, Instruments, Structures, Seaplanes, etc. 63*s.* (64*s.* 9*d.*)

1940 Aero and Hydrodynamics, Aerofoils, Airscrews, Engines, Flutter, Icing, Stability and Control Structures, and a miscellaneous section. 50*s.* (51*s.* 9*d.*)

1941 Aero and Hydrodynamics, Aerofoils, Airscrews, Engines, Flutter, Stability and Control Structures. 63*s.* (64*s.* 9*d.*)

1942 Vol. I. Aero and Hydrodynamics, Aerofoils, Airscrews, Engines. 75*s.* (76*s.* 9*d.*)
Vol. II. Noise, Parachutes, Stability and Control, Structures, Vibration, Wind Tunnels. 47*s.* 6*d.* (49*s.* 3*d.*)

1943 Vol. I. Aerodynamics, Aerofoils, Airscrews. 80*s.* (81*s.* 9*d.*)
Vol. II. Engines, Flutter, Materials, Parachutes, Performance, Stability and Control, Structures. 90*s.* (92*s.* 6*d.*)

1944 Vol. I. Aero and Hydrodynamics, Aerofoils, Aircraft, Airscrews, Controls. 84*s.* (86*s.* 3*d.*)
Vol. II. Flutter and Vibration, Materials, Miscellaneous, Navigation, Parachutes, Performance, Plates and Panels, Stability, Structures, Test Equipment, Wind Tunnels. 84*s.* (86*s.* 3*d.*)

1945 Vol. I. Aero and Hydrodynamics, Aerofoils. 130*s.* (132*s.* 6*d.*)
Vol. II. Aircraft, Airscrews, Controls. 130*s.* (132*s.* 6*d.*)
Vol. III. Flutter and Vibration, Instruments, Miscellaneous, Parachutes, Plates and Panels, Propulsion. 130*s.* (132*s.* 3*d.*)
Vol. IV. Stability, Structures, Wind Tunnels, Wind Tunnel Technique. 130*s.* (132*s.* 3*d.*)

Annual Reports of the Aeronautical Research Council—

1937 2*s.* (2*s.* 2*d.*) 1938 1*s.* 6*d.* (1*s.* 8*d.*) 1939–48 3*s.* (3*s.* 3*d.*)

Index to all Reports and Memoranda published in the Annual Technical Reports, and separately—

April, 1950 - - - - R. & M. 2600 2*s.* 6*d.* (2*s.* 8*d.*)

Author Index to all Reports and Memoranda of the Aeronautical Research Council—

1909—January, 1954 R. & M. No. 2570 15*s.* (15*s.* 6*d.*)

Indexes to the Technical Reports of the Aeronautical Research Council—

December 1, 1936—June 30, 1939	R. & M. No. 1850	1*s.* 3*d.* (1*s.* 5*d.*)
July 1, 1939–June 30, 1945	R. & M. No. 1950	1*s.* (1*s.* 2*d.*)
July 1, 1945—June 30, 1946	R. & M. No. 2050	1*s.* (1*s.* 2*d.*)
July 1, 1946—December 31, 1946	R. & M. No. 2150	1*s.* 3*d.* (1*s.* 5*d.*)
January 1, 1947—June 30, 1947	R. & M. No. 2250	1*s.* 3*d.* (1*s.* 5*d.*)

Published Reports and Memoranda of the Aeronautical Research Council—

Between Nos. 2251–2349	R. & M. No. 2350	1*s.* 9*d.* (1*s.* 11*d.*)
Between Nos. 2351–2449	R. & M. No. 2450	2*s.* (2*s.* 2*d.*)
Between Nos. 2451–2549	R. & M. No. 2550	2*s.* 6*d.* (2*s.* 8*d.*)
Between Nos. 2551–2649	R. & M. No. 2650	2*s.* 6*d.* (2*s.* 8*d.*)

Prices in brackets include postage

HER MAJESTY'S STATIONERY OFFICE

York House, Kingsway, London W.C.2; 423 Oxford Street, London W.1 (Post Orders: P.O. Box 569, London S.E.1); 13a Castle Street, Edinburgh 2; 39 King Street, Manchester 2; 2 Edmund Street, Birmingham 3; 109 St. Mary Street, Cardiff; Tower Lane, Bristol, 1; 80 Chichester Street, Belfast, *or through any bookseller.*

S.O. Code No. 23-3045

R. & M. No. 3045